Genetic screening for single-cell variability modulators driving therapy resistance

Eduardo A. Torre[1], Eri Arai[3,*], Sareh Bayatpour[2,*], Lauren E. Beck[2], Benjamin L. Emert[6], Sydney M. Shaffer[2,5], Ian A. Mellis[6], Krista A. Budinich[3], Ashani Weeraratna[4], Junwei Shi[3,**], Arjun Raj[2,3,7,**,***]

[1] Biochemistry and Molecular Biophysics Graduate Group, Perelman School of Medicine, University of Pennsylvania, Philadelphia, PA
[2] Department of Bioengineering, School of Engineering and Applied Science, University of Pennsylvania, Philadelphia, PA
[3] Department of Cancer Biology, Perelman School of Medicine, University of Pennsylvania, Philadelphia, PA
[4] The Wistar Institute, Philadelphia, PA
[5] Department of Pathology and Laboratory Medicine, Perelman School of Medicine, University of Pennsylvania, Philadelphia, PA
[6] Genomics and Computational Biology Graduate Group, Perelman School of Medicine, University of Pennsylvania, Philadelphia, PA
[7] Department of Genetics, Perelman School of Medicine, University of Pennsylvania, Philadelphia, PA
*Equal contribution
**Co-corresponding authors
***Lead contact

Abstract:
Non-genetic fluctuations in the molecular state of a cell can lead to different cell fate choices in response to environmental perturbations. In the context of cancer, such fluctuations can lead to the formation of rare cells within the population that are able to survive treatment with targeted therapies. However, the biological processes governing the formation of these cells and their subsequent impact on therapy resistance remains largely unknown. We performed genetic screens using CRISPR/Cas9 to identify over 80 factors that modulate these rare cell fluctuations. These screens revealed several novel targets affecting cellular variability and, in turn, therapy resistance. Transcriptomic analysis revealed that many of these novel targets appeared to act via distinct mechanisms from those previously identified; for instance, knockout of either *DOT1L* or *LATS2* appeared to increase resistance by increasing the degree of cellular differentiation, as opposed to knockout of *MITF* or *SOX10*, which achieve the same effect by decreasing cellular differentiation. We show that the timing of inhibition of these new variability-altering factors can affect the degree of resistance to targeted therapies. Our results suggest that cellular plasticity may be subject to regulatory processes that play critical roles in cell fate determination.

Introduction

The advent of therapies designed to inhibit particular oncogenic targets has raised the potential to cure certain cancers. However, while these therapies are able to kill most of the tumor cells, often a few cells remain that are able to ultimately repopulate the tumor (Garraway and Jänne 2012; Trunzer et al. 2013). There are numerous mechanisms by which these rare cells become

resistant. While these mechanisms are often genetic in origin, for instance a mutation affecting the site of action of the drug, non-genetic variability between otherwise identical cells has emerged as another mechanism by which cells can be rendered resistant (Sharma et al. 2010; Gupta et al. 2011; Pisco and Huang 2015; Shaffer et al. 2017, 2018; Cohen et al. 2008; Weinreb et al. 2018; Rambow et al. 2018; Su et al. 2017). A commonality in the study of genetic versus non-genetic resistance mechanisms is the goal of determining the molecular "state" of a cell that confers distinct ultimate fates such as death or therapy resistance—a mutation in the case of genetic mechanisms versus high levels of expression of particular marker genes in the case of non-genetic mechanisms. However, a critical difference is that while genetic mutations largely arise through spontaneous, stochastic processes, non-genetic fluctuations can in principle occur due to the changes in activity of specific biological pathways, yielding the potential to enhance or inhibit the formation of these rare cells by targeting those pathways specifically. Yet, to date, little is known about pathways that affect non-genetic rare-cell variability, leaving their therapeutic potential unrealized.

As an example, in melanoma, several groups have identified transient rare-cell populations within otherwise homogeneous cells that are able to proliferate in the face of treatment with $BRAF^{V600E}$ inhibitors (Fallahi-Sichani et al. 2017; Tirosh et al. 2016; Rambow et al. 2018; Shaffer et al. 2017; Torre et al. 2018). These cells, which we refer to as pre-resistant cells, are often marked by transiently high expression of several resistance marker genes, such as *EGFR*, *NGFR* and *AXL*. When drug is added to enriched populations of these cells, they are far more likely to be drug resistant than other cells in the population (Shaffer et al. 2017) (Fig. 1A, top). Furthermore, once these cells are exposed to drug, they are reprogrammed such that the transient pre-resistant phenotype is converted to a stably drug-resistant phenotype characterized by massive changes in signaling and gene expression profiles.

These results serve as an example of linking the molecular state of the cell (before the addition of the drug) to the eventual fate of the cell (upon adding drug) (Symmons and Raj 2016; Raj and van Oudenaarden 2008; Raj et al. 2010; Wernet et al. 2006; Süel et al. 2007; Maamar, Raj, and Dubnau 2007; Mojtahedi et al. 2016; Rambow et al. 2018). This mapping from cellular state to phenotypic fate has two key components. One is the fluctuations that give rise to distinct cellular states in the original population. The other is conversion of that molecular difference into a distinct phenotypic fate; in this case, the biological processes that convert a pre-resistant cell into a stably resistant colony. We were interested in dissecting the molecular regulators of this mapping.

With the advent of CRISPR/Cas9 technology, it is now possible to perform genetic screens to identify regulators of various molecular processes. For therapy resistance, virtually all screens have been designed to detect changes to cellular fate only—i.e., changes in the final number of resistant cells, typically measured as a proliferation phenotype (Shalem et al. 2014; Konermann et al. 2014; Strub et al. 2018; Joung et al. 2017). However, the non-genetic paradigm of drug resistance consists of multiple processes, specifically first the aforementioned transient fluctuations in single cells that results in the generation of many cellular states within an

otherwise homogeneous population, and then the subsequent drug-induced selection and reprogramming (Shaffer et al. 2017). Each of these processes may in principle have distinct regulatory mechanisms, and so the opportunity remains to direct screening techniques at these specific aspects of non-genetic drug resistance; for instance to identify factors that affect the initial fluctuations in the cellular state (Fig. 1A, middle). These factors may then also affect the overall degree of drug resistance, but potentially through new, previously undiscovered mechanisms that allow for new therapeutic targets that affect drug resistance in ways not revealed by classical resistance screens.

We here describe the results of genetic screens designed to capture modulators of single cell state variability that subsequently affect cell fate decisions. Specifically, in the context of melanoma, we performed pooled CRISPR/Cas9 genetic screens to reveal modulators of the rare cell state we have previously identified as being responsible for drug resistance. We recover several factors known to play key roles in melanoma, and also identify several new factors. Using RNA sequencing to measure the transcriptome profiles induced by knocking out these factors, these factors organized into a few distinct functional classes, suggesting that these sets of factors may affect cell state variability and consequently cell fate selection through a small number of distinct modes. Drugs targeting these new orthogonal mechanisms display a variety of synergistic effects when coupled with therapy, sometimes depending on the relative timing of drug application.

Results

CRISPR/Cas9 genetic screens identify factors that modulate cellular states

We wanted to identify factors that affected the fluctuations in cellular state that lead to single cells being resistant to drug. We took advantage of a clonal melanoma cell line (WM989 A6-G3) that we have extensively characterized as exhibiting resistance behavior in cell culture that is broadly comparable to that displayed in patients. Phenomenologically, in cell culture, we observe that upon addition of a roughly cytostatic dose of the $BRAF^{V600E}$ inhibitor vemurafenib (1μM), the vast majority of cells die or stop growing, but around 1 in 2,000-3,000 cells continues to proliferate, ultimately forming a resistant colony after 2-3 weeks in culture in vemurafenib. We have previously demonstrated that before the application of drug, there is a rare subpopulation of cells (pre-resistant cells) that express high levels of a number of markers, and that these cells are far more likely to be resistant than other cells (Shaffer et al. 2017). In order to identify modulators of the fluctuations that lead to the formation of this subpopulation of pre-resistant cells, we designed a large scale loss-of-function pooled CRISPR genetic screen (which we dubbed the “state screen”) comprised of ~13,000 single guide RNAs (sgRNAs) targeting functionally relevant domains of ~2,000 proteins, with roughly six distinct single guide RNAs per

domain (1402 transcription factors targets, 481 kinase targets, 176 epigenetic targets; each single guide RNA targets an important functional domain, see Supplemental tables 1-3) (Huang et al. 2018; Tarumoto et al. 2018; Brien et al. 2018). To conduct the screen, we stably integrated *Streptococcus pyogenes* Cas9 (spCas9) into the WM989-A6-G3 cell line, creating the line WM989-A6-G3-Cas9, and isolated a single cell clone, which we refer to as WM989-A6-G3-Cas9-5a3. We verified that this cell line was capable of editing the genome and that it still contained pre-resistant cells marked by the expression of drug-resistance markers (Supplemental fig. 1).

Our screening strategy consisted of first transducing the pooled library of single guide RNAs into a population of cells using lentivirus at a low multiplicity of infection. Given that the pre-resistant cells show up only rarely within the population, we needed to ensure that we had sufficient cell numbers in order to effectively sample differences in the frequency of pre-resistant cells. Thus we expanded the culture to maintain around 50,000-250,000 total cells per each individual single guide RNA, for a total of roughly a billion cells per screen. We then used a combination of magnetic sorting and flow cytometry to isolate cells that were positive for both EGFR and NGFR expression, both of which are prominent markers of the pre-resistant rare cell subpopulation. We then sequenced the single guide RNAs in this sorted subpopulation to determine which single guide RNAs were over- or under-represented as compared to the unsorted total population. Here, over-representation suggests that knockout of the gene leads to an increased frequency of $NGFR^{HIGH}/EGFR^{HIGH}$ cells and vice versa (Fig. 1B). To select “hits” from the screen, we designed a series of criteria to identify and rank targets (see methods for a detailed description of the selection criteria). For ranking targets, we considered a target in the screen to be a Tier 1 “hit” if we detected a two-fold change in abundance for ≥ 75% of the single guide RNAs (Tier 2 ≥ 66%, Tier 3 ≥ 50%, Tier 4 < 50%).

By these criteria, we obtained a set of 61 targets identified as factors (Tier 1 or Tier 2) affecting the frequency of $NGFR^{HIGH}/EGFR^{HIGH}$ cells in our screen (Fig. 2, Supplemental table 4). Of these, 25 increased the frequency of $NGFR^{HIGH}/EGFR^{HIGH}$ cells, while 36 decreased the frequency. Reassuringly, many genes known to be important factors in melanoma biology emerged from our screen, including *SOX10* and *MITF*, both of which are key melanocyte transcription factors whose downregulation is often associated with increased drug resistance (Sun et al. 2014; Almeida et al. 2019; Hartman and Czyz 2015; Wellbrock and Arozarena 2015). Other tumor suppressors include *RUNX3*, whose expression is often lost in melanoma (Kitago et al. 2009; Bae and Choi 2004) and *LATS2*, a regulator of the Hippo pathway (Harvey, Zhang, and Thomas 2013).

Additionally, several new factors not previously associated with resistance to $BRAF^{V600E}$ inhibition emerged from our screen. These include genes such as *DOT1L*, which encodes an H3K79 methyltransferase associated with melanoma oncogenesis (Zhu et al. 2018), and *BRD2*, which encodes a protein that is a member of the BET family, often overexpressed in human melanoma (Segura et al. 2013).

In order to assess the robustness and generality of our results, we performed secondary, targeted screens in WM989-A6-G3-Cas9 (non-clonal) cells as well as in another $BRAF^{V600E}$ human melanoma cell line, 451Lu-Cas9. This screen included sgRNAs targeting 34 of the Tier 1 and 2 factors we identified in the state screen, as well as another 52 factors from Tiers 3 and 4 (these lower confidence hits may also have been Tier 1 or 2 hits in the "fate" screen described below; Supplemental table 5). We found that 25 of the 34 high confidence hits showed at least a two fold change in the frequency of $NGFR^{HIGH}/EGFR^{HIGH}$ cells concordant with the effects detected in the original screening clonal cell line (WM989-A6-G3-Cas9-5a3). In 451Lu-Cas9 cells, 20 of the 34 targets also showed a change in the frequency of $NGFR^{HIGH}/EGFR^{HIGH}$ cells, with 11 of those exhibiting at least a two-fold change, indicating that the factors identified by our screen are likely general and that our results are not entirely dependent on the specific cellular context of the original WM989-A6-G3-Cas9-5a3 cell line (Supplemental Fig. 3, Supplemental table 4). Not all the factors were validated by this secondary screen, which may be due to technical challenges associated with performing screens for rare cell phenotypes (see discussion). Also, even Tier 4 hits displayed qualitative agreement in these secondary screens, although quantitatively they were not as strong as the effects of the Tier 1 and 2 hits, suggesting that our screen has isolated many strong effect hits but that there may be several additional factors with smaller effect sizes that we were unable to detect.

A cell survival "fate" screen reveals a distinct set of factors that modulate drug resistance

Our variability "state" screen is conceptually distinct from more conventional resistance screen designs for which the screened phenotype is overall survival and proliferation in the face of drug. Our hypothesis was that those more conventional screens would identify a different set of factors because the underlying biological processes may be different. To test this hypothesis, we also performed a parallel, conventional genetic screen for resistance to find modulators that specifically altered cellular "fate"; i.e., formation of resistant colonies when exposed to $BRAF^{V600E}$ inhibition. Here, we used the same cells and the same library of single guide RNAs, but instead of isolating $NGFR^{HIGH}/EGFR^{HIGH}$ cells, we added vemurafenib and grew the cells until large resistant colonies formed, at which point we isolated DNA and sequenced it to look for over- and under-represented single guide RNAs as before (Fig. 3A). Here, if a single guide RNA is overrepresented in the resistant cell population, it means that knocking out the gene it targets resulted in an increase in the number of cells that survive the drug and acquire resistance, and vice versa for under-representation of single guide RNAs.

As before, we ranked the targets into tiers based on the percent of single guide RNAs that exhibited at least a two-fold change in representation throughout the screen (Tier 1, ≥ 75%; Tier 2, ≥ 66%; Tier 3, ≥ 50%; Tier 4, < 50%). We identified 24 factors (Tier 1 and 2) that emerged as hits from our fate screen (Fig. 3B, Supplemental table 4). Among those, there were a number of factors that affect or act downstream of signaling pathways such as MAPK (CSK) (Okada et al. 1991), Wnt/B-catenin (*KDM2A*)(Lu et al. 2015), and Hippo (*LATS2*) (Harvey, Zhang, and

Thomas 2013). Of these, 20 of the 24 emerged as predicted enhancers of the number of resistant cells, while the remaining 4 were predicted to decrease the number of resistant cells. Of all 24 hits, five were also identified by our state screen (Fig. 3C).

The lack of correspondence between the two screens most likely reflects the fact that distinct biological processes may play a more dominant role in either single cell variability or other aspects of the overall acquisition of resistance. If it were possible to run the screen for overall acquired resistance to saturation—i.e., isolate all possible factors affecting resistance—then we would in principle be able to find all variability factors that affected the resistance phenotype as well. However, bottlenecks in the screening process owing to the rarity of the resistance phenotype at the single cell level meant that some factors (e.g. *CSK*) may come to dominate the fate screen, making it difficult to fully capture all factors through just the conventional resistance screen alone.

As with the state screen, we also performed a secondary, targeted fate screen in both WM989-A6-G3-Cas9 and 451Lu-Cas9 cells to test for the generality of the factors we had identified. This time we included nine of the top factors affecting vemurafenib resistance in our screen (as well as 77 targets that either affected vemurafenib resistance but did not pass the thresholds to be called a hit, or affected the frequency of $NGFR^{HIGH}$/$EGFR^{HIGH}$ cells, see Supplemental table 5). In WM989-A6-G3-Cas9, we found that seven of the nine targets replicated the effect that we observed originally. For 451Lu-Cas9, the same seven factors showed similar effects, suggesting again that the factors isolated may not be specific to the cellular context (Supplemental fig. 4).

Factors affecting variability also affect overall drug resistance to different degrees

We designed our state screen to identify factors that increase or decrease the percentage of $NGFR^{HIGH}$/$EGFR^{HIGH}$cells. The implicit assumption was that increasing the percentage of $NGFR^{HIGH}$/$EGFR^{HIGH}$ cells would be associated with an increase in the number of cells that went on to acquire drug resistance. However, EGFR and NGFR are, in this context, just markers of the pre-resistant state, and most of the factors identified in the state screen did not appear in our fate screen for factors affecting overall resistance. Thus, it was conceivable that factors identified from our screen might simply affect the transcriptional regulation of these genes but not affect the frequency of cells being in the pre-resistant state *per se*. Thus, we conducted extensive validation experiments to demonstrate that: 1. the factors identified actually did change the frequency of cells expressing NGFR as predicted by the screen, and then 2. that these changes in the frequency of $NGFR^{HIGH}$ cells translated into changes in the number of resistant colonies upon application of vemurafenib.

To measure the frequency of $NGFR^{HIGH}$ cells, we generated a population of ≥ 500 cells in which the target of interest had been edited and then performed immunofluorescence using antibodies

that bound to NGFR (86 different targets, each targeted at least three times using different sgRNA designs for a total of ~288 different samples including controls). Most of the targets selected from the state screen showed an increase or decrease in the number of NGFR^{HIGH}cells concordant with the effect on the primary screen, with 21 of 34 tier one and tier two targets showing at least a 50% increase or decrease over control (Fig. 4A-B). NGFR immunofluorescence performed on cells in which targets from tiers three and four were knocked out also seemed to confirm the effect measured in the primary screen, but to a lesser extent, with only 21 out of 49 targets increasing or decreasing the frequency of NGFR^{HIGH} cells by 50% or more (Fig. 4B, tiers 3 and 4; Supplemental fig. 5). This confirmed that our screen was able to identify factors that modulated the expression of the pre-resistance marker NGFR, and further suggests that there are likely additional factors with moderate-to-small effect size that our screen was unable to detect reliably. (Note that we also organized the targets tier in the fate screen and show their effect on the frequency of NGFR^{HIGH} cells in the bottom panel of Fig. 4B.)

We next took a subset of these knockout populations (33 different targets, 21 of which are tier 1 or tier 2 hits from the primary state screen), added vemurafenib, and counted the number of resistant colonies after three weeks in drug. Despite not being classified as a tier 1 or 2 hit in the primary fate screen, we found that 15 of the 21 factors tested showed an increase or decrease in the number of resistant colonies, consistent with the prediction that an increased or decreased percentage of NGFR^{HIGH} cells would lead to a concomitant change in resistance (Fig. 4A, C, Supplemental fig. 6). We also tested seven tier 1 and tier 2 targets from the primary fate screen, six of which led to a change in the number of colonies resistant to vemurafenib (Fig. 4C, right panel; Supplemental fig. 6-7). Additionally, for DOT1L, where small molecule inhibitors exist, we confirmed that at non-cytotoxic doses of the drug, inhibition of this target led to dramatic changes in the number of colonies able to survive and proliferate upon BRAF^{V600E} inhibition (Supplemental fig. 8). Furthermore, DOT1L inhibition led to an increase in the number of resistant colonies not only upon targeting BRAF^{V600E}, but also upon MEK inhibition and simultaneous MEK and BRAF^{V600E} inhibition (Supplemental fig. 9).

If the level of *NGFR* expression perfectly reflected the probability of a cell becoming resistant upon addition of drug, then changes in the number of resistant colonies should be directly proportional to changes in the number of NGFR^{HIGH} cells. However, while the general trend indicated such a pattern, knockouts of individual genes varied widely in the degree to which this relationship held (Fig. 4D). For instance, knockout of *EP300* resulted in a ~two-fold increase in the number of NGFR^{HIGH} cells but only a small increase in the number of resistant colonies, while knockout of *CSK* resulted in only a small increase in the number of NGFR^{HIGH} but had at least a six-fold increase in the number of resistant colonies. (Importantly, the number of colonies for the CSK knockout is an underestimate due to difficulties in accurately counting colonies in highly-confluent plates, see Supplemental fig. 10 for raw image of colonies.) This is probably why CSK was a dominant hit in our screen for full resistance for vemurafenib. Conceptually, a change in the number of resistant colonies without a proportional change in the number of NGFR^{HIGH} cells could result from a change in the mapping between state and fate induced by the drug (perhaps best thought of as a change in “threshold”), or from a shift in the distribution

of the internal state of the cells that is not reflected in a change in NGFR expression. While our results cannot conclusive resolve this difference, some of our results argue in favor of changes to the mapping between state and fate itself. For instance, the *CSK* knockout cell line showed an increase in the number of resistant colonies but also an increase in the number of resistant cells that do not form colonies (Supplemental fig. 10). This suggested that, in addition to the usual pre-resistant cells that form colonies, an additional set of cells in the *CSK* knockout line were now enabled to survive drug. This suggests that the "threshold" for cells to survive drug may have changed; i.e., the state-fate mapping has been altered by the removal of *CSK*.

Transcriptomics reveals multiple mechanisms for cellular state and fate modulation

Our screens revealed a large number of factors affecting pre-resistance and full resistance (state and fate) that act across a range of biological processes, including a variety of signaling pathways and transcriptional regulatory mechanisms. Interestingly, *a priori*, no particular pathways appeared to dominate the set of identified factors; however it was possible that seemingly unrelated genes nevertheless affect pre-resistance and resistance through common biological processes.

To look for such pathways, we used RNA sequencing to measure genome-wide transcript abundance levels for 266 knockout cell lines targeting 85 different proteins (each targeted with 2-3 separate single guide RNAs; see supplementary table 4). These 85 proteins included 34 targets selected from the state screen, nine selected from the fate screen (five of these nine targets overlapped with 34 hits from the state screen), with the remaining targets being tier 3 and tier 4 targets in the primary screens. (Also, of the 85 protein targets, 45 validated by testing for changes in the frequency of $NGFR^{HIGH}$ cells by immunofluorescence and/or changes in the number of resistant colonies upon adding vemurafenib; Fig. 4, Supplemental figs. 5 and 7.)

Initially, we clustered the transcriptome profiles from the different cell lines, including only genes differentially expressed in at least one sample (Supplemental fig. 11). We found that while the transcriptomes induced by some gene knockouts were clearly distinct (such as *MITF*, *SOX10* and *KDM1A*), many others appeared to coalesce and show relatively small differences, despite the fact that our validation results showed that these knockouts exhibited qualitatively different effects on resistance. We thus reasoned that while the sets of genes whose expression changes in our knockouts may be non-overlapping, these genes could still belong to similar categories of biological processes; i.e., different knockouts may all affect different genes all within a common pathway, for instance differentiation. Thus, using the transcriptome of each knockout, we performed a gene set enrichment analysis (GSEA, see methods) and obtained an enrichment score for a number of biological processes from the Gene Ontology terms database (Fig. 5)(Subramanian et al. 2005). Using these enrichment scores, the knockout lines clustered in a more obvious pattern. Notable clusters include *MITF* and *SOX10*, as before, which formed a distinct cluster from e.g. *DOT1L*, *LATS2*, *RUNX3* and *GATA4*, which form a cluster with a

rather opposing transcriptome profile. This latter cluster primarily consists of genes whose knockout results in an increase in vemurafenib resistant colonies. Interestingly, knockout or downregulation of *MITF* and *SOX10* are also well known in the literature to increase drug resistance (Sun et al. 2014; Rambow et al. 2018), although by an apparently distinct mechanism in this context. (Note that the role of *MITF* in therapy resistance in general is complex (Bai, Fisher, and Flaherty 2019).

The clusters we identified also seem to correspond to distinct phenotypic profiles, meaning the resultant changes in the frequency of $NGFR^{HIGH}$ cells and number of resistant colonies. For instance, the transcriptomes of the knockouts in cluster 1 seem to mimic many aspects of the transcriptomes of $NGFR^{HIGH}$, $EGFR^{HIGH}$, $NGFR^{HIGH}/EGFR^{HIGH}$, and even vemurafenib resistant melanoma cells (Fig. 5A). Knockout of these targets showed a strong correspondence between the frequency of $NGFR^{HIGH}$ cells and the number of colonies that developed under BRAF inhibition, suggesting that the increase/decrease in the frequency of pre-resistant cells was the cause of increased/decreased resistance. Often, this relationship was relatively proportional, as was the case for the knockout of *LATS2, JUNB, FOSL1,* and *CBFB*; Fig. 5B). For *MITF* and *SOX10*, however, the relationship between the frequency of $NGFR^{HIGH}$ cells and the number of resistant colonies was much weaker, with very large changes in the latter but not the former. Accordingly, our transcriptomic analysis suggests that these knockouts lead to changes in gene expression that are distinct from those of $NGFR^{HIGH}/EGFR^{HIGH}$ cells.

Principal components analysis of the enrichment scores indeed showed that these two categories of genes whose knockout affects resistance are diametrically opposed in their profile (Fig. 6). The gene set categories associated with the transcriptome differences for these knockouts are largely related to development, differentiation, morphogenesis, and migration (see Supplemental table 6). This fits with the fact that reduction of the master differentiation factors *MITF* and *SOX10* leads to decreased differentiation and hence drug resistance, but the other cluster of knockouts points to a potentially novel means by which to increase drug resistance by instead *increasing* the expression of genes involved in differentiation (via knockout of *DOT1L*, *LATS2*, *RUNX3*, etc.).

The transcriptome analysis also revealed different categories of knockouts that resulted in a reduction of the number of resistant colonies. Some resistance reducing knockouts (*BRD8* and *PRKAA1*) clustered with *DOT1L*, while another *BRD2* clustered with *MITF/SOX10*. It is possible that these factors work in inverse ways to reduce drug resistance by either affecting differentiation or dedifferentiation. Meanwhile, the majority of resistance reducing knockouts appeared to cluster separately into two distinct clusters, generally through changes in the expression of a distinct set of genes. For one cluster (cluster 2), the set of genes whose expression was affected included several associated with metabolism (e.g. RNA transport and biosynthesis of amino acids), suggesting that modulation of metabolic processes may be a means of reducing drug resistance (Supplemental table 6). The other cluster did not show any coherent set of biological processes affected (e.g. *SRC*, *IRF7*, *PKN2*, among others), rendering that particular pathway or set of pathways rather mysterious.

Relative timing of targeting variability can affect drug resistance

Our two screens, one for variability in cellular state (pre-resistance) and the other for the ultimate cellular fate (stable drug resistance), isolated different factors, and our transcriptomic profiles suggest that different factors may act by different pathways. One possibility is that the effects of inhibiting these factors in concert with the standard $BRAF^{V600E}$ inhibitor may vary, in particular, with respect to the relative timing of drug administration. For instance, if a factor primarily affected the mapping between initial state and ultimate fate, then it may be that pre-administration of the drug would have no effect on resistance, but co-administration with the $BRAF^{V600E}$ inhibitor would have a synergistic effect. We previously observed this with the EGFR inhibitor, where inhibition of EGFR before the inhibition of $BRAF^{V600E}$ had no effect, but concurrent inhibition greatly reduced the number of resistant colonies (Shaffer et al. 2017). In principle, the opposite may also be true: if a factor affected primarily the initial state of the cell but did not greatly affect the mapping between state and fate, then inhibition of the factor before $BRAF^{V600E}$ inhibition may have a strong effect on ultimate resistance, but if applied concurrently with $BRAF^{V600E}$ inhibition, it may have a greatly reduced effect because the $BRAF^{V600E}$ inhibitor already selects which cells will survive before the internal state of the cell can change.

To test for such a possibility, we used the DOT1L inhibitor pimenostat (Daigle et al. 2011; Basavapathruni et al. 2012) (which increases the number of colonies resistant to vemurafenib over a range of doses; Supplemental fig. 8) to see if timing of DOT1L inhibition would affect the formation of resistant colonies. In addition to the standard vemurafenib treatment, we both pre-treated with the DOT1L inhibitor for seven days before adding vemurafenib and co-treated with the DOT1L inhibitor concurrently with vemurafenib (we tested both pre-treatment followed by vemurafenib alone and pre-treatment followed by concurrent treatment). We found that pre-inhibition of DOT1L resulted in three-fold more colonies than with $BRAF^{V600E}$ inhibition alone, but that co-treatment with the DOT1L and $BRAF^{V600E}$ inhibitors led to no change in the number of resistant colonies (Fig. 7), suggesting that DOT1L inhibition is altering the distribution of states of the cells, and consequently the number of cells that develop resistance to $BRAF^{V600E}$ inhibition. Our results demonstrate that the relative timing of inhibition of different pathways can have a profound effect on resistance.

Discussion

We have here demonstrated, using high-throughput screening, that there are genetic factors that can alter cellular plasticity in cancer cells, thereby affecting their resistance to targeted therapeutics. We identified several such factors, including known players in the biology of melanoma such as *MITF* and *SOX10*, but also a variety of new factors that appear to work by distinct, indeed potentially opposing pathways from these. These factors revealed new possible vulnerabilities that a conventional genetic screen targeting resistance did not uncover, thus

demonstrating the potential for screens specifically designed to target single cell variability to reveal new biological mechanisms that may subsequently emerge as therapeutic opportunities. Drug screens targeting gene expression “noise” have also shown similar therapeutic potential (Dar et al. 2014).

While we isolated several new factors that specifically affected cellular variability, it is important to note that no single factor we isolated resulted in a change in cellular variability that was stronger than all the rest; i.e., no factor emerged as the “smoking gun”. This may be the result of the fact that our screen did not target all potential regulators. Alternatively, it may be that the biology of cellular variability is intrinsically multifactorial, with the coherent activity of many factors being required for cells to ultimately enter the highly deviated cellular state responsible for phenotypes like drug resistance (Shaffer et al. 2018). Larger scale screens may help reveal a more complete picture of the origins of rare cell behavior; however, the limitations imposed by the rarity of the pre-resistant cellular phenotype make this rather difficult. The raw numbers of cells required to properly sample these rare cell behaviors in a pooled genetic screening format remains a major technical challenge for the field of rare cell biology.

Indeed, it is the very difficulty of performing these screens at full depth that provides motivation for screening for variability rather than simply screening for resistance. If one is primarily interested in factors affecting resistance, then in principle such a screen, if carried to saturation, would reveal all such factors, including those that exert such an effect via modulation of cellular variability. However, the degree of overlap in the factors identified between our variability screen and our conventional resistance screen was relatively small. This lack of overlap suggests that distinct biological processes may dominate the results of these differently designed screens. That of course in turn raises the question of why one might want to perform variability screens at all, given that the phenotype of interest is resistance. Our results on timing of variability inhibition suggest that while the mechanisms governing rare cell variability may not appear as potent as those revealed by conventional resistance screens, the fact that they represent *distinct* mechanisms means that they may present an opportunity to be used in tandem. It is also possible that these mechanisms may be more dominant in other, more clinically relevant contexts.

In our validation studies, for several factors, we measured the effects of knocking out those factors on both the number of $NGFR^{HIGH}$ cells (which serves as a proxy for cellular state) and number of resistant colonies upon adding vemurafenib (which is our measurement for cellular fate). Interestingly, different knockouts affected both of these validation metrics differently, with some (e.g. *LATS2*) both increasing the frequency of $NGFR^{HIGH}$ cells as well as concomitantly increasing the number of resistant cells, and some (e.g. *CSK*) dramatically increasing the frequency of resistant cells without a proportional change in the frequency of $NGFR^{HIGH}$ cells. One possible way to conceptualize these distinct phenotypic outcomes is that the former category of knockout affects primarily cellular variability, i.e., cellular state, while the latter affects the mapping between these states and their fates upon addition of vemurafenib. In one simple model, one could imagine a distribution of cellular states in the initial population and a

threshold whereby cells above the threshold are resistant and those below the threshold are not (Supplemental fig. 12). In this model, some knockouts may alter the distribution of cells in the initial population, thus rendering a different proportion of them above or below the threshold, or may alter the threshold itself, or potentially some combination of both. It is wise to caution against this simple interpretation, however. First, we note that NGFR expression is just a marker for the pre-resistant state, and it may be that factors may affect the frequency of pre-resistant cells without showing any effect on NGFR expression, thus giving the false appearance of a change in the mapping. (Arguing against this, however, is the fact that the transcriptomes of knockouts such as *DOT1L* that increase the frequency of NGFR and resistance appear to be similar to the profile of $NGFR^{HIGH}$ cells themselves; Fig. 5) Further molecular profiling of individual cells from these knockouts may help reveal the ways in which the molecular state of these cells changes. Secondly, it is also likely that the categorization of fates as “resistant” or “dead” is dramatically oversimplified, and that there may be a number of different types of resistant cells (anecdotally, we have noticed that the resistant cells in some of our knockout lines do appear morphologically different from those formed in the unperturbed cell line). Such results suggest that there is a mapping from a continuum of initial cellular states to multiple, canalized, or even potentially continuous cellular fates. An important future direction is to characterize this mapping and its regulation.

In this study, we have focused on cellular variability in the context of drug resistance in cancer. However, we have observed similar rare-cell variability in primary melanocytes (Shaffer et al. 2017), raising the possibility that the same variability may play a role in normal biological processes as well. It is thus possible that the factors we have isolated may play a role in regulating variability in these normal biological contexts, and it remains to be seen whether such factors act primarily in melanocytes or act more generally across different cell types in various tissues.

Methods

Cell Culture

We obtained patient-derived melanoma cells (WM989 and 451Lu, female and male, respectively) from the lab of Meenhard Herlyn. For WM989 we derived a single cell subclone (A6-G3) in our lab (Shaffer et al. 2017). We grew these cells at 37°C in Tu2% media (78% MCDB, 20% Leibovitz’s L-15 media, 2% FBS, and 1.68mM CaCl2). We authenticated all cell lines via Human STR profiling. We periodically tested all cell lines for mycoplasma infections.

Plasmid Construction and single guide RNA Cloning

All the Cas9 positive melanoma cell lines in this study were derived by lentiviral transduction with a Cas9 expression vector (EFS-Cas9-P2A-Puro, Addgene: 108100). All the single guide RNAs were cloned into a lentiviral expression vector LRG2.1(Addgene: #108098), which contains an optimized single guide RNA backbone. The annealed single guide RNA oligos were T4 ligated to the BsmB1-digested LRG2.1 vector. To improve U6 promoter transcription

efficiency, an additional 5' G nucleotide was added to all single guide RNA oligo designs that did not already start with a 5' G.

Construction of Domain-Focused single guide RNA Pooled Library

Gene lists of transcription factors (TF), kinases, and epigenetic regulators in the human genome were manually curated based on the presence of DNA binding domain(s), kinase domains, and epigenetic enzymatic/reader domains. The protein domain sequence information was retrieved from NCBI Conserved Domains Database. Approximately 6 independent single guide RNAs were designed against individual DNA binding domains (Supplementary tables 1-3).(Huang et al. 2018; Tarumoto et al. 2018; Brien et al. 2018) The design principle of single guide RNA was based on previous reports and the single guide RNAs with the predicted high off-target effect were excluded (Hsu et al., 2013). For the initial pooled CRISPR screen, all of the single guide RNAs oligos including positive and negative control single guide RNAs were synthesized in a pooled format (Twist Bioscience) and then amplified by PCR. PCR amplified products were cloned into BsmB1-digested LRG2.1 vector using Gibson Assembly kit (NEB#E2611). For the targeted pooled validation screen, individual single guide RNAs were synthesized, cloned, and verified via Sanger sequencing in a 96-well array platform (Supplementary table 5). Individual single guide RNAs were pooled together in an equal molar ratio. To verify the identity and relative representation of single guide RNAs in the pooled plasmids, a deep-sequencing analysis was performed on a MiSeq instrument (Illumina) and confirmed that 100% of the designed single guide RNAs were cloned in the LRG2.1 vector and the abundance of >95% of individual single guide RNA constructs was within 5-fold of the mean (data not shown).

Lentivirus preparation

We produced lentivirus containing single guide RNAs using HEK293T cells cultured in DMEM supplemented with 10% Fetal Bovine Serum and 1% penicillin/streptomycin. When the cells reached 90-100% confluency, we mixed the single guide RNA vectors with the packaging vector psPAX2 and envelope vector pVSV-G in a 4:3:2 ratio in OPTI-MEM (ThermoFisher Scientific: #31985070) and polyethylenimine (PEI, Polysciences: #23966). We collected viral supernatants for up to 72 hours twice daily.

Transduction of spCas9

We introduced the stable expression of spCas9 via spinfection of lentivirus along with 5ug/ml polybrene for 25 minutes at 1750 rpm. We exchanged the media ~6 hours post-transduction and selected for cells expressing spCas9 via puromycin selection (1-2μg/ml, 1 week). For WM989-A6-G3, we generated two cell lines, WM989-A6-G3-Cas9 and WM989-A6-G3-Cas9-5a3, the later being a single cell isolate of the bulk Cas9-expressing population. We generated a 451Lu-Cas9 cell line from 451Lu cells.

Transduction of lentivirus containing single guide RNAs

For transfection of melanoma cells, we infected cells with lentivirus and 5ug/ml polybrene for 25 minutes at 1750 rpm. We exchanged the media ~6 hours post-transfection. We quantified the percent of the population transfected by measuring the number of GFP-positive cells at day 5

post-transfection. For the screens, we aimed to transfect 30% of the population. For all other experiments, we aimed to transfect >95% of the population.

Primary pooled CRISPR screens

We worked with three main pooled single guide RNA libraries in WM989-A6-G3-Cas9-5a3 cells. These libraries targeted ~2,000 different kinases, transcription factors, and proteins involved in epigenetic regulation. In total, the libraries contained ~13,000 different single guide RNAs including non-targeting and cell-viability editing controls (Supplementary tables 1-3). We aimed to transfect > 1,000 cells per single guide RNA and isolated ~1,000 cells per single guide RNA about a week post-transfection and prior to any selection. These baselines allowed us to validate the efficiency of our screen by single guide RNA enrichment/depletion of non-targeting controls and of controls that affect cell viability (Supplemental fig. 2). Additionally, these baselines helped us identify single guide RNAs with lethal effects in our cells. Given that we were interested in rare cell phenotypes that exist in 1:2000 cells or less, throughout our screens we significantly expanded the population of cells to 50,000-250,000 cells per single guide RNA, often surpassing a billion cells per screen. This scale allowed us to observe the rare cell phenotypes dozens-to-hundreds of times in each of our controls (and in each of our single guide RNAs).

The state screen aimed to identify perturbations that altered the frequency of $NGFR^{HIGH}/EGFR^{HIGH}$ cells. To this end, one month after we transfected and expanded the cells, we isolated the $NGFR^{HIGH}/EGFR^{HIGH}$ cells via magnetic cell sorting (MACS) followed by fluorescence-activated cell sorting (FACS) (see below). We also collected an additional ~1,000 cells per single guide RNA, without any selection, for comparison. Then, we isolated DNA from the cells and built sequencing libraries (see below) to quantify the representation of each single guide RNA in the $NGFR^{HIGH}/EGFR^{HIGH}$ population and compare it to the unsorted baseline.

In the fate screen we aimed to identify proteins important for the development of resistance to vemurafenib. Here, we treated the cells as above, except that instead of isolating $NGFR^{HIGH}/EGFR^{HIGH}$ cells we grew cells resistant to vemurafenib (see below) by exposing the cells to vemurafenib for three weeks. As above, we isolated DNA from the resulting population of cells and built sequencing libraries to quantify the representation of each single guide RNA. The raw output of all screens was reads per single guide RNA.

To select hits in our screens, we first normalized the output of our screens to reads per million, and then calculated the fold change in single guide RNA representation between different samples. For our state screen, we focused on the fold change in single guide RNA representation between $NGFR^{HIGH}/EGFR^{HIGH}$ cells and the bulk population of melanoma cells. For the fate screen, we focused on the fold change in single guide RNA representation between cells treated for three weeks with 1μM vemurafenib (a $BRAF^{V600E}$ inhibitor) and cells never exposed to the drug. After normalizing the change in single guide RNA representation of each single guide RNA by the median change across all single guide RNAs, we organized our hits into tiers (one through four) based on the percent of single guide RNAs against the target

exhibiting at least a two-fold change in representation. We considered hits those targets where (1) ≥ 66% of its single guide RNAs showed at least a two-fold enrichment enrichment/depletion throughout the screen, and (2) no two single guide RNAs showed a significant change (two-fold change) in opposing directions (i.e. one single guide RNA is significantly enriched in the selected population while another one is significantly depleted). Note that we excluded from analysis any single guide RNA with less than 10 raw reads in all samples.

Secondary, targeted pooled CRISPR screen

To validate the replicability and generality of our hits, we designed a pool of single guide RNAs for targeted screening that targeted proteins that either emerged as hits in our primary screens or did not pass our hit-selection criteria but changed the frequency of $NGFR^{HIGH}/EGFR^{HIGH}$ cells or the frequency of cells resistant to vemurafenib (Supplemental table 5). In this pool, we included ~3 single guide RNAs per protein target, and carried out the screen in WM989-A6-G3-Cas9-5a3 cells as well as in another $BRAF^{V600E}$ melanoma cell line, 451Lu-Cas9. As before, we conducted a state screen where we isolated $NGFR^{HIGH}/EGFR^{HIGH}$ cells as well as a fate screen where we exposed cells to 1μM vemurafenib for three weeks. Here too, we first normalized the output of our screens to reads per million, and then calculated the fold change in single guide RNA representation between different samples. Unlike on our primary screens, here we normalized the change in single guide RNA representation to the median change in representation of the ten non-targeting single guide RNAs controls included in the screen.

Immunostains

For NGFR stain of fixed cells, after fixation and permeabilization, we washed the cells for 10 min with 0.1% BSA-PBS, and then stained the cells for 10 min with 1:500 anti-NGFR APC-labelled clone ME20.4 (Biolegend, 345107). After two final washes with PBS we kept the cells in PBS. For EGFR and NGFR stains of live cells, we incubated melanoma cells in suspension for 1 hour at 4C with 1:200 mouse anti-EGFR antibody, clone 225 (Millipore, MABF120) in 0.1% BSA PBS. We then washed twice with 0.1% PBS-BSA and then incubated for 30 minutes at 4C with 1:500 donkey anti-mouse IgG-Alexa Cy3 (Jackson Laboratories, 715-545-150). We washed the cells again (twice) with 0.1% BSA-PBA and incubated for 10 minutes with 1:500 anti-NGFR APC-labelled clone ME20.4 (Biolegend, 345107). We again washed the cells twice with 0.1% BSA-PBS and finally re-suspended them in 1%BSA-PBS.

Isolation of pre-resistant cells (MACS + FACS)

To enrich for $NGFR^{HIGH}/EGFR^{HIGH}$ cells we first immunostained melanoma cells as detailed above. Then, we used a Manual Separator for Magnetic Cell Isolation (MACS, with LS columns and Anti-APC microbeads). In short, following the manufacturer's instructions, we incubated cells and microbeads at 4C for 15 min, then washed and pelleted the cells via centrifugation. After resuspending the cells, we passed them through LS magnetic columns. After enriching for $NGFR^{HIGH}$ cells, we proceeded to select only the cells expressing both NGFR and EGFR via Fluorescent-Activated Cell Sorting (FACS, MoFlo Astrios EQ).

Growth of resistant colonies
To grow melanoma cells resistant to $BRAF^{V600E}$ inhibition, we exposed melanoma cells to 1μM vemurafenib (PLX4032, Selleckchem S1267) for 2-3 weeks. For the $BRAF^{V600E}$ and MEK co-inhibition assays, we also used dabrafenib at 500nM and 100nM (GSK2118436, Selleckchem S2807), trametinib at 5nM and 1nM (GSK1120212, Selleckchem S2673), and cobimetinib at 10nM and 1nM (GDC-0973, Selleckchem S8041).

Inhibition of DOT1L via small molecule inhibitor
For all assays involving pharmacological inhibition of DOT1L we used pinometostat at concentrations ranging from 1μM to 5μM (EPZ5676, Selleckchem S.7062).

MiSeq library construction and sequencing
In order to quantify the single guide RNA representation following selection in our screen we sequenced the single guide RNAs as per (Shi et al. 2015). In short, we isolated genomic DNA using the Quick-DNA Midiprep Plus Kit (Zymo Research: #D4075) per manufacturer specifications. We then PCR-amplified the single guide RNAs using Phusion Flash High Fidelity Master Mix Polymerase (Thermo Scientific: #F-548L) and primers that incorporate a barcode and a sequencing adaptor to the amplicon. Our amplification strategy consisted of an initial round of parallel PCRs (23-29 cycles of up to 200 parallel reactions per sample. We then pooled the PCR reactions and purified them using the NucleoSpin® Gel and PCR Clean-up kit (Macherey-Nagel: #740609.250). We continued with eight PCR cycles using Phusion Flash High Fidelity Master Mix Polymerase, followed by column purification with the QIAquick PCR Purification Kit (QIAGEN: #28106). We quantified the single guide RNA libraries with the DNA 1000 Kit (Agilent: #5067-1504) on a 2100 Bioanalyzer Instrument (Agilent: #G2939BA). We pooled the barcoded single guide RNA libraries and sequenced via 150-cycle paired-end sequencing (MiSeq Reagent Kit v3, Illumina: #MS-102-3001). We then mapped the resulting sequences to our reference single guide RNA library and proceeded to select hits.

Cell fixation and permeabilization
For our imaging assays we fixed cells for 10 min with 4% formaldehyde and permeabilized them with 70% ethanol overnight.

Colony formation assays
For each condition tested, we first plated cells in duplicate (~10-50,000 cells per well of a 6-well plate). We fixed and permeabilized one of the duplicates to use as a baseline and exposed the second duplicate to the test condition. At the endpoint, we fixed and permeabilized the second duplicate.

Image analysis of NGFR immunostains
We developed a custom MATLAB pipeline for counting cells and quantifying immunofluorescence signal of DAPI-stained and NGFR-stained cells (https://bitbucket.org/arjunrajlaboratory/rajlabscreentools/src/default/). The software stitches together a large tiled image, then uses DAPI to identify cells. Using the nuclear area, it then

looks at a set of pixels near the nucleus to quantify fluorescence intensity of the NGFR staining. After quantifying the expression level of NGFR following knockout of select screen targets and of non-targeting controls, we quantified the minimum expression level needed to be considered an $NGFR^{HIGH}$ cell. First, we selected the top one percent highest expressors of NGFR in each of our non-targeting negative controls. Then, within that top one percent we obtained the median expression level of the lowest expressor across all controls, and used that as a threshold to quantify the frequency of $NGFR^{HIGH}$ cells in each of our knockout samples. Then, we calculated the change in frequency of $NGFR^{HIGH}$ cells in each test condition compared to controls and obtained a median fold change and standard deviation across all samples with knockout of one same protein (~3 different biological samples per protein). In total, we targeted ~86 different proteins across ~258 different knockout biological samples.

Image analysis of colony formation

We developed a custom MATLAB pipeline for counting cells and colonies in tiled images of DAPI-stained cells (https://bitbucket.org/arjunrajlaboratory/colonycounting_v2/src/default/). First, the software stitches the individual image tiles into one large image by automatically (or with user input) determining the amount of overlap between each individual image. Then, the software identifies the location of each cell in the stitched image by searching for local maxima. We then manually identify the colony boundaries and quantify the number of colonies in each sample. We then calculate the frequency of resistant colonies by dividing the number of colonies by the total number of cells present in culture prior to $BRAF^{V600E}$ inhibition. Finally, we scale the frequency of colonies to colonies per 10,000 cells and calculate the change in frequency between each sample and the median change across controls.

RNA-sequencing and identification of differential expression

We sequenced mRNA in bulk from WM989-A6-G3 and WM989-A6-G3-Cas9 populations as per Shaffer et. al. In addition to quantifying the transcriptome of $EGFR^{HIGH}$cells, $NGFR^{HIGH}$, $NGFR^{HIGH}$/$EGFR^{HIGH}$ cells and vemurafenib-resistant cells, we quantified the transcriptional changes following the knockout of many tier 1 and tier 2 hits from both the state and fate screens. In addition to hits from our screens, we also quantified the transcriptome of targets that were not tier1 or tier2 hits, but show a change in the frequency of $NGFR^{HIGH}$/$EGFR^{HIGH}$ cells or of cells resistant to vemurafenib. In total, we targeted ~85 different proteins, each in triplicate (using different single guide RNAs) for a total of 280+ RNA sequencing samples. For each sample, we isolated mRNA and built sequencing libraries using the NEBNext Poly(A) mRNA Magnetic Isolation Module and NEBNext Ultra RNA Library Prep Kit for Illumina per manufacturer instructions. We then sequenced the libraries via paired-end sequencing (36x2 cycles) on a NextSeq 500. We aligned reads to hg19 and quantified reads per gene using STAR and HTSeq. We then used DEseq2 to identify differentially expressed genes.

Gene set enrichment analysis

To identify “biological signatures” enriched or depleted following the knockout of a given target we used the GSEA software (http://software.broadinstitute.org/gsea/index.jsp) in combination

with several of the MSigDB gene sets. In particular, we focused in the Biological Process ontology of the Gene Ontology gene sets (http://geneontology.org) to obtain enrichment scores.

Grouping of targets based on transcriptomic analysis

To group targets into classes based on their transcriptional effects, we clustered all RNA-seq samples (hierarchical clustering via pheatmap in R) based on the change in expression (as obtained by DEseq2) of any gene differentially expressed (two-fold change over control, with an adjusted p value ≤ 0.05) in at least one of the 85+ knockouts. We also grouped targets via pheatmap based on the enrichment scores obtained via GSEA. Additionally, we identified the genes in each knockout driving the enrichment score (leading edges) and identified the KEGG pathways and Gene Ontology terms enriched for those genes via cluster profiler. Finally, to identify the axes that account for the variability between each knockout we also performed principal component analysis based on the gene set enrichment scores of each knockout. Note that in the aforementioned analysis we included the transcriptomes of pre-resistant cells (marked by the expression of EGFR alone, NGFR alone, and NGFR and EGFR in combination) and of cells resistant to vemurafenib.

Supplemental Tables

All tables can be found at:
https://www.dropbox.com/sh/t08558cl4mepfm6/AABBvbtlTPSNNPoMC9NTro-9a?dl=0
-Supplemental table 1. - sgRNA sequences of primary screens - Epigenetic targets
-Supplemental table 2. - sgRNA sequences of primary screens - Kinase targets
-Supplemental table 3. - sgRNA sequences of primary screens - Transcription factor targets
-Supplemental table 4. - Master table with results from genetic screens and their follow up experiments
-Supplemental table 5. - Targets included secondary screen
-Supplemental table 6. - Enrichment analysis of leading edges

Software and data availability

All data and code used for the analysis can be found at
https://www.dropbox.com/sh/t08558cl4mepfm6/AABBvbtlTPSNNPoMC9NTro-9a?dl=0
The software used for colony growth image analysis can be found at:
https://bitbucket.org/arjunrajlaboratory/colonycounting_v2/src/default/ . The software used for analysis of immunofluorescence images can be found at:
https://bitbucket.org/arjunrajlaboratory/rajlabscreentools/src/default/

Acknowledgements

We want to thank Dr. Meenhard Herlyn for always providing excellent advice and guidance. We also thank the Flow Cytometry core, especially Florin Tuluc, at CHOP for all their advice and help. We also thank all members of the Raj Lab as well as John Murray for their comments and suggestions. We thank C. Vakoc for providing the TF, epigenetic regulator, and kinase domain-focused sgRNA library. J.S acknowledges support from Linda Pechenik Montague Investigator Award and Cold Spring Harbor Laboratory sponsored research. AR acknowledges

NIH/NCI PSOC award number U54 CA193417, NSF CAREER 1350601, P30 CA016520, SPORE P50 CA174523, NIH U01 CA227550, NIH 4DN U01 HL129998, NIH Center for Photogenomics (RM1 HG007743), and the Tara Miller Foundation. AW acknowledges support from CA207935 and CA174746. AW acknowledge support from CCSG P30CA010815 and NIH U01 CA227550.

Declaration of interests

A.R. and S.M.S. receives patent royalty income from LGC/Biosearch Technologies related to Stellaris RNA FISH probes. All other authors declare no competing interests

Author contributions

E.T., J.S., and A.R. designed and supervised the study. E.T. performed the experiments and analysis. E.A., K.B. assisted with CRISPR screens. S.B. assisted with tissue culture, image acquisition, and analysis. L.B. designed image analysis software. B.E, S.S. assisted with acquisition of transcriptomic data. B.E, S.S., I.M. assisted with data analysis. A.W. provided guidance on interpretation of the data.

Figure legends

Figure 1. Pooled CRISPR screen design to identify modulators of cellular state and fate in the context of drug resistance to targeted therapies in melanoma.

A. (top) In melanoma, the initial molecular profile (i.e., “state”) of a cell within an otherwise homogeneous population, indicated by green vs. gray coloring of cell, dictates the ultimate fate of the cell (e.g. proliferation vs. death). Changing the number of cells in a given state (A, middle) or the mapping between state and fate (A, bottom) can alter the number of resistant colonies that form upon addition of the $BRAF^{V600E}$ inhibitor vemurafenib.

B. We designed a pooled CRISPR screen to detect modulators of the rare cellular states that lead to drug resistance. After transducing a library of single guide RNAs and expanding the population, we isolated cells with high expression of both NGFR and EGFR, then sequenced the single guide RNAs to determine which gene knockouts alter the frequency of these cells. Changes in the frequency of a given single guide RNA in this population (e.g. targets A and C) indicate that these targets may affect the frequency of $NGFR^{HIGH}$/$EGFR^{HIGH}$ cells in the population, and thus may affect the cellular state associated with pre-resistance.

Figure 2. Factors identified as altering rare cellular states associated with pre-resistance.

A. After transducing a population of melanoma cells and isolating $NGFR^{HIGH}$/$EGFR^{HIGH}$ cells (see Fig. 1B), we quantified the frequency of each single guide RNA in the resulting population. Our screening scheme utilized three separate pooled single guide RNA libraries, one targeting epigenetic domains (top left), another targeting kinases (bottom left), and a final one targeting transcription factors (right). We organized the targets within each single guide RNA library by biological process. (While a given target could fall into several categories, each target is

assigned to a single group and plotted only once.) Each dot represents a single guide RNA, grouped by gene target (5-6 single guide RNAs per target), with the $\log_2$ fold change representing the number of times the single guide RNA was detected in the sorted population versus an unsorted population of melanoma cells transduced with the same library. For display purposes, all single guide RNAs with fold changes beyond the axis limits were placed at the edge of the axis as indicated. For targets considered "hits" by our rubric (see methods), we highlighted the single guide RNA dot by the color assigned to that biological process. Non-targeting controls correspond to single guide RNAs not targeting any loci in the genome. Cell viability controls target proteins required for cell survival and proliferation, but not specifically associated with rare-cell behavior. Supplemental fig. 2 details the effect of these editing controls throughout the screen.

Figure 3. Screen for factors modulating number of resistant colonies upon BRAF^{V600E} inhibition (cellular "fate").

A. We performed a pooled CRISPR screen to detect modulators of cellular fate (e.g. number of drug-resistant colonies) in the presence of BRAF^{V600E} inhibitors. After transducing a library of single guide RNAs and expanding the population, we exposed the cells to the BRAF^{V600E} inhibitor vemurafenib (1μM) for 3 weeks, after which we sequenced the single guide RNAs in the surviving population. Changes in the frequency of detection of a given single guide RNA indicates that its target may affect the ability of a cell to survive and proliferate upon BRAF^{V600E} inhibition.

B. After transfecting a population of melanoma cells we exposed them to vemurafenib (BRAF^{V600E} inhibitor, 1μM) for three weeks to grow resistant colonies. We then sequenced the DNA to quantify the single guide RNA representation of each target in the resulting population, using the same libraries as in Fig. 2. For a more detailed description see methods section.

C. Effect overlap between state and fate hits. For each target (dots) its position represents the number of times (as median log2 fold change) the single guide RNAs were detected in the NGFR^{HIGH}/EGFR^{HIGH} population vs. an unsorted population of melanoma cells (state screen, x-axis), or in the population of cells resistant to vemurafenib vs. the population of cells prior to treatment (fate screen, y-axis). Orange labels correspond to Tier 1 and Tier 2 targets in the state screen; blue corresponds to Tier 1 and Tier 2 targets in the primary fate screen; purple corresponds to targets that are Tier 1 or Tier 2 in both screens. The effects of all targets in both screens is displayed as a density histogram.

Figure 4. Validation of effects on state and fate of variability hits by via NGFR immunofluorescence and resistant colony formation.

A. To validate the phenotypic effect of targets identified by our genetic screen, we knocked out 86 of the targets and after knocking out the gene, we quantified both the frequency of NGFR^{HIGH} cells by immunofluorescence using anti-NGFR antibodies (top) and the number of resistant colonies (bottom) that form upon BRAF^{V600E} inhibition. Here we show example state and fate validation of BRD2 and LATS2 knockouts. The schematic represents the effect of the knockout in the primary state screen on the frequency of NGFR^{HIGH}/EGFR^{HIGH} cells.

B. Frequency of $NGFR^{HIGH}$ cells following the knockout of select targets. Each bar represents the change in the number of $NGFR^{HIGH}$ cells following knockout of the gene indicated over replicates, each using a different single guide RNA. Error bars represent the standard error of the mean across the replicates. We carried out each measurement over three replicates, but excluded samples with low cell density (< 500 cells). The star above or below the bars indicate targets where, after excluding samples with low cell numbers, n = 1. Tiers refers to the degree of confidence we have in each particular hit, with tier 1 representing highest confidence hits for which ≥ 75% of the single guide RNAs passed a threshold of two-fold change in the primary state screen. We performed this analysis for hits from both the state screen (top) and the fate screen (bottom).
C. Resistance phenotype of melanoma cells following the knockout of hits from the primary screens. Each bar represents the $\log_2$ fold change over non-targeting control in the number colonies able to grow in vemurafenib following knockout of the gene indicated. The number of colonies for each target is normalized to the number of cells present in culture before $BRAF^{V600E}$ inhibition, reported as number of colonies per every 10,000 cells in culture prior to treatment (see methods). As before, the different tiers represent the percent of single guide RNAs against a given target exhibiting at least a two-fold change throughout the primary (left) state or (right) fate screens. On the left panel, we highlight in green and gray the effect a given target has in the frequency of $NGFR^{HIGH}$/$EGFR^{HIGH}$ cells (based on the primary state screen). On the right panel, we highlight in red and gray the effect a given target has in the number of cells that resist $BRAF^{V600E}$ inhibition (based on the primary fate screen). In this plot each bar represents one experimental replicate. See Supplemental fig. 6 for replicates.
D. Relationship between the frequency on $NGFR^{HIGH}$ cells (x-axis) and the number of resistant colonies (y-axis). We plot the frequency of $NGFR^{HIGH}$ cells as the mean $\log_2$ fold change over three replicates in the number of $NGFR^{HIGH}$ cells following knockout of the gene indicated normalized by cells with non-targeting sgRNAs. (For variability of the effect size across replicates of a given target, see Fig. 4B). We quantified the $\log_2$ fold change in the number of resistant colonies in the knockout cell line as compared to the non-targeting control cell lines. Orange points are targets identified as tier 1 or tier 2 hits in the primary state screen; blue are those identified as tier 1 or tier 2 hits in the primary fate screen; purple are those identified as tier 1 or tier 2 hits in both state and fate screen; gray, those that may have shown an effect in either or both screens, but were not classified as tier 1 or tier 2 in either screen.

Figure 5. Gene set enrichment analysis of the transcriptional effects induced by the knockout of select screen targets.
A. The heatmap represents biclustering analysis of different knockout cell lines (rows) based on the Gene Set Enrichment Analysis score of Gene Ontology gene sets (Biological process GO terms, columns in heatmap). Red indicates enrichment in the sense that there are more differentially upregulated genes in knockout vs. control in that gene set than expected by chance, whereas blue indicates enrichment of downregulated genes (shade indicates degree of enrichment). Each target knockout (rows) represents transcriptomes of biological triplicates (unless otherwise stated on Supplemental table 4). Target labels (rows) in green indicate genes whose knockout increased the frequency of $NGFR^{HIGH}$/$EGFR^{HIGH}$ cells in the primary screen,

while red indicates targets whose knockout increased the number of cells resistant to vemurafenib, and gray indicates targets that decreased the frequency of either $NGFR^{HIGH}$/$EGFR^{HIGH}$ cells or of cells resistant to vemurafenib. As before, we organized targets into tiers indicated by the number of asterisks next to the label (Tier 1, ****; Tier 2, ***; Tier 3, **; Tier4, *), based on the percent of single guide RNAs against that target that showed at least a two-fold change in the primary screen (see knockout color key). Based on the dendrogram on the left, we group targets into six clusters. The white boxes inside the heatmap highlights groups of gene sets specifically upregulated in a given cluster.
B. Relationship between the frequency on $NGFR^{HIGH}$ cells (x-axis) and the number of resistant colonies (y-axis). As in Fig. 4D, we plot the frequency of $NGFR^{HIGH}$ cells as the median log_2 fold change over three replicates in the number of $NGFR^{HIGH}$ cells following knockout of the gene indicated normalized by cells with non-targeting single guide RNAs. (For variability of the effect size across replicates of a given target, see Fig. 4B). We quantified the log_2 fold change in the number of resistant colonies in the knockout cell line as compared to the non-targeting control cell lines. We color-coded all targets by groupings based on their transcriptomes (see Fig. 5A) following knockout of the gene indicated.

Figure 6. Principal component analysis of the transcriptional effects induced by the knockout of select screen targets. We performed principal component analysis of the transcriptional effects induced by the knockout of select screen targets. We used as input the gene set enrichment scores from Fig. 5A to identify primary axes that account for the greatest degree of transcriptome variability across knockout cell lines. In A and B, the color indicates the effect of the knockout in either the primary state screen (A), or in the primary fate screen (B). The size of the dot indicates the degree of confidence we have in each particular hit, with tier 1 representing highest confidence hits for which ≥ 75% of the single guide RNAs passed a threshold of two-fold change in the primary state screen. In black we highlight melanoma cells where we did not knockout any targets but either enriched for $EGFR^{HIGH}$ cells, $NGFR^{HIGH}$ cells, $EGFR^{HIGH}$/$NGFR^{HIGH}$ cells, or for cells resistant to vemurafenib.

Figure 7. Effect of timing of DOT1L inhibition on the development of resistance to $BRAF^{V600E}$ inhibition.
A. To assess the effect of DOT1L inhibition (green arrows, pinometostat at 4μM) at different times on a cell's ability to survive $BRAF^{V600E}$ inhibition, we first established a baseline number of colonies that grow when WM989-A6-G3 cells are exposed to 1μM of vemurafenib for three weeks (leftmost panel). Then, in a separate population, we either inhibited $BRAF^{V600E}$ and DOT1L simultaneously (co-treatment), inhibited DOT1L first (seven days) and then $BRAF^{V600E}$ (three additional weeks; pre-treatment), or inhibited DOT1L before (seven days) and during three weeks of vemurafenib treatment (pre-treatment and co-treatment).
B. Number of resistant colonies that result from each therapeutic regimen in Fig. 7A as a the mean fold change over baseline (vemurafenib alone) for three replicates normalized to the number of cells in culture prior to $BRAF^{V600E}$ inhibition. Error bars indicate the standard error of the mean over triplicates.

Supplemental figure 1. Technical validation of WM989-A6-G3-Cas9-5a3 cell line.
A. WM989-A6-G3-Cas9-5a3 cells expressing NGFR, EGFR, and both NGFR and EGFR are more likely to survive and proliferate in the presence of vemurafenib (Shaffer et al. 2017). Here, we show the number of colonies that grow upon vemurafenib exposure in a mixed population of WM989-A6-G3-Cas9-5a3 or in the same population but enriched for $EGFR^{HIGH}$ cells, $NGFR^{HIGH}$ cells, or $NGFR^{HIGH}/EGFR^{HIGH}$ cells.
B. Single guide RNA representation over time (as percent GFP-positive cells) in WM989-A6-G3 cells with or without Cas9 expression. Negative controls are single guide RNAs aimed at ROSA26, a non-expressing gene in human melanoma. Positive controls target proteins necessary for cell viability. Only cells expressing both Cas9 and a positive control single guide RNA should disappear from the population over time.

Supplemental figure 2. Effect of negative and positive control single guide RNAs in the primary CRISPR screens. Our primary pooled CRISPR screen included non-targeting single guide RNAs as negative controls (gray bars, 50+ single guide RNAs) as well as single guide RNAs affecting cell viability as positive controls (red bars, 25+ single guide RNAs). We quantified the change in representation of these single guide RNAs over time and report the fold change in representation from six days after transfection to right before selection (vemurafenib exposure or selection by NGFR and EGFR expression). We expect positive controls to lose representation over time more often than negative controls. Our screening scheme utilized three separate pooled single guide RNA libraries, one targeting kinases (top), another targeting epigenetic domains (middle), and a final one targeting transcription factors (bottom).

Supplemental figure 3. Secondary validation of hits across multiple cell lines by targeted CRISPR screening.
A. We assessed the robustness and generality of the effect of hits identified in the primary state screen (WM989-A6-G3-Cas9-5a3, black bars) by carrying out a secondary screen containing single guide RNAs for only a subset of our targets (see Supplemental table 5 for list of targets). We carried out this screen in WM989-A6-G3-Cas9 (orange bars) as well as in another $BRAF^{V600E}$ melanoma cell line (451Lu-Cas9, blue). We organized the targets by tiers (tiers 1-4) based on the fraction of single guide RNAs against a given target exhibiting at least a two-fold change throughout the primary screen (Tier 1, ≥ 75%; Tier 2, ≥ 66%; Tier 3, ≥ 50%; Tier 4, < 50%), thus corresponding to the degree of confidence we have in the hit. Within each tier, names highlighted in green correspond to targets whose single guide RNAs are enriched in $NGFR^{HIGH}/EGFR^{HIGH}$ cells in the primary screen and gray represents targets whose single guide RNAs are underrepresented in these rare cells. We plotted the median $\log_2$ fold change in single guide RNA representation (normalized by non-targeting controls) across three single guide RNAs. Error bars represent the standard deviation of the fold change across all single guide RNAs for a given target. Dotted error bars in red extend beyond the limits of the graph. Note that the limits of the axes vary between tiers.

Supplemental figure 4. Secondary validation of hits across multiple cell lines by targeted CRISPR screening.

A. We assessed the robustness and generality of the effect of hits identified in the primary fate screen (WM989-A6-G3-Cas9-5a3, black bars) by carrying out a secondary screen containing single guide RNAs for only a subset of our targets (see Supplemental table 5 for list of targets). We carried out this screen in WM989-A6-G3-Cas9 (orange bars) as well as in another $BRAF^{V600E}$ melanoma cell line (451Lu-Cas9, blue). We organized the targets by tiers (tiers 1-4) based on the fraction of single guide RNAs against a given target exhibiting at least a two-fold change throughout the primary screen (Tier 1, ≥ 75%; Tier 2, ≥ 66%; Tier 3, ≥ 50%; Tier 4, < 50%), thus corresponding to the degree of confidence we have in the hit. Within each tier, names highlighted in red correspond to targets whose single guide RNAs are enriched in cells resistant to vemurafenib in the primary screen and gray represents targets whose single guide RNAs are underrepresented in these cells. We plotted the median $\log_2$ fold change in single guide RNA representation (normalized by non-targeting controls) across three single guide RNAs. Error bars represent the standard deviation of the fold change across all single guide RNAs for a given target. Dotted error bars in red extend beyond the limits of the graph. Note that the limits of the axes vary between tiers.

Supplemental figure 5. Percent of targets from the primary state screen that validate. To assess the sensitivity of our screen, we validated the effect observed in the primary state screen for a select group of targets via NGFR immunofluorescence. Here, each dot represents an individual single guide RNA, and we plot the change in single guide RNA representation between $NGFR^{HIGH}/EGFR^{HIGH}$ cells and controls (as measured in the primare state screen). We then organize all sgRNAs into tiers (y-axis, tiers one through four) based on the percent of single guide RNAs against a target showing at least a two-fold change in representation on $NGFR^{HIGH}/EGFR^{HIGH}$ cells. In red we highlight targets that when tested again produced at least a 50% change in the frequency of $NGFR^{HIGH}$ cells. In black we highlight those target that we tested but did not validate, and in gray we show those target we did not test. We display the percent of genes tested and validated at each tier on the right.

Supplemental figure 6. Validation of effects on fate of variability hits by resistant colony formation. Resistance phenotype of melanoma cells following the knockout of hits from the primary screens. Each bar represents the $\log_2$ fold change over non-targeting control in the number colonies able to grow following knockout of the gene indicated. The number of colonies for each target is normalized to the number of cells present in culture before $BRAF^{V600E}$ inhibition, reported as number of colonies per every 10,000 pre-treatment cells (see methods). As before, the different tiers represent the percent of single guide RNAs against a given target exhibiting at least a two-fold change throughout the primary (top) state or (bottom) fate screens. On the top panel, we highlight in green and gray the effect a given target has in the frequency of $NGFR^{HIGH}/EGFR^{HIGH}$ cells (based on the primary state screen). On the bottom panel, we highlight in red and gray the effect a given target has in the number of cells that resist $BRAF^{V600E}$ inhibition (based on the primary fate screen). In this plot each bar represents one experimental replicate (distinct from the one in Fig. 4C).

Supplemental figure 7. Percent of targets from the primary fate screen that validate. To assess the sensitivity of our screen, we validated the effect observed in the primary fate screen for a select group of targets via colony formation assays. Here, each dot represents an individual single guide RNA, and we plot the change in single guide RNA representation between cells resistant to vemurafenib and cells that have never been exposed to the drug (as measured in the primary fate screen). We then organize all single guide RNAs into tiers (y-axis, tiers one through four) based on the percent of single guide RNAs against a target showing at least a two-fold change in representation on drug resistant cells. In red we highlight targets that when tested again produced at least a 50% change in the frequency colonies resistant to $BRAF^{V600E}$ inhibition. In black we highlight those target that we tested but did not validate, and in gray we show those target we did not test. We display the percent of genes tested and validated at each tier on the right.

Supplemental figure 8. Effect of pharmacological inhibition of DOT1L on resistance to $BRAF^{V600E}$ inhibition.
A. Resistance phenotype of melanoma cells following pharmacological inhibition of DOT1L. We pre-treated melanoma cells for seven days with either DMSO, or various concentrations of the DOT1L inhibitor pinometostat (EPZ5676). Then, we exposed the cells to 1μM vemurafenib for three weeks.
B. To assess the effect of DOT1L inhibition on cellular proliferation, we the compared the population size of WM989-A6-G3 cells over time treated with either 4μM of pinometostat (DOT1L inhibitor) or with DMSO. The population size is estimated by the amount of nucleic acids present in the population using a CyQuant GR dye. The values represent mean fluorescence signal over triplicates. Error bars represent standard error of the mean.

Supplemental figure 9. Effect of DOT1L inhibition on resistance to $BRAF^{V600E}$ and MEK inhibition therapy. Resistance phenotype of melanoma cells to BRAF and MEK inhibitors following pharmacological inhibition of DOT1L. We pre-treated melanoma cells for seven days with either DMSO or 4μM of pinometostat. We then exposed the cells to one of two $BRAF^{V600E}$ inhibitors (vemurafenib and dabrafenib, left panels), to one of two MEK inhibitors (cobimetinib and trametinib, middle panels), or to a combination of a $BRAF^{V600E}$ and MEK inhibitor (vemurafenib + cobimetinib; dabrafenib + trametinib, right panels). White arrows point to a few of the many colonies that grew under each condition.

Supplemental figure 10. Effect of CSK knockout on a cell's ability to develop resistance to $BRAF^{V600E}$ inhibition. To assess the effect of CSK on the development of resistance to vemurafenib, we plated CSK-knockout WM989-A6-G3-Cas9-5a3 cells and exposed them to 1μM vemurafenib for three weeks. As before, after the treatment we counted the number of resulting colonies and compared it to the number of colonies resulting from WM989-A6-G3-Cas9-5a3 cells without the knockout. Note that the number of resistant cells in the CSK sample is too large to accurately identify individual colonies. We only counted colonies we could clearly delineate, and thus, the number of colonies reported is an underestimate.

Supplemental figure 11. Clustering analysis of the transcriptional effects induced by knockout of select screen targets. The heatmap represents the biclustering analysis of different screen targets (rows) based on the change in expression of all genes differentially expressed in at least one knockout (columns). Within the heatmap, red indicates an increase in expression following the knockout, while blue indicates a decrease in gene expression (see heatmap color key). Each targets (rows) represents transcriptomes of biological triplicates (unless otherwise stated on Supplemental table 4). Target labels (rows) in green indicate genes whose knockout increased the frequency of $NGFR^{HIGH}/EGFR^{HIGH}$ cells in the primary screen. In red are those whose knockout increased the number of cells resistant to vemurafenib, and in gray are those that decreased the frequency of either $NGFR^{HIGH}/EGFR^{HIGH}$ cell or of cells resistant to vemurafenib. As before, we organized targets into tiers indicated by the number of asterisks, based on the percent of single guide RNAs against that target that showed an effect in the primary screen (see knockout color key).

Supplemental figure 12. Model of adaptation thresholds and cellular heterogeneity in the development of resistance to targeted therapies. Variability in the expression of various markers are associated with an individual cell's probability to survive drug treatment. In one simple model, cellular variability occurs along a single ordinate, which can be conceptualized as the degree of "greenness". Operationally, this may be related to the expression of a marker of pre-resistance, such as *NGFR*. In this model, there is a threshold (red line, top panel) that divides cells along this axis into those that adapt to the drug and become resistant vs. those that no longer proliferate when challenged with drug. Here, there are at least two ways by which one could conceivably alter the number of cells that survive the drug. In one scenario (middle) the distribution of "greenness" could change, leading to more cells being above the threshold, leading to more resistant colonies. In another scenario, the distribution of phenotypes remains unchanged, but the threshold itself moves, also leading to more resistant colonies. Our results suggest (but do not prove) that both scenarios may play out to varying degrees as a result of different genes being knocked out.

Citations

Almeida, Filipe V., Stephen M. Douglass, Mitchell E. Fane, and Ashani T. Weeraratna. 2019. "Bad Company: Microenvironmentally Mediated Resistance to Targeted Therapy in Melanoma." *Pigment Cell & Melanoma Research* 32 (2): 237–47.

Bae, Suk-Chul, and Joong-Kook Choi. 2004. "Tumor Suppressor Activity of RUNX3." *Oncogene* 23 (24): 4336–40.

Bai, Xue, David E. Fisher, and Keith T. Flaherty. 2019. "Cell-State Dynamics and Therapeutic Resistance in Melanoma from the Perspective of MITF and IFNγ Pathways." *Nature Reviews. Clinical Oncology*, April. https://doi.org/10.1038/s41571-019-0204-6.

Basavapathruni, Aravind, Lei Jin, Scott R. Daigle, Christina R. A. Majer, Carly A. Therkelsen, Tim J. Wigle, Kevin W. Kuntz, et al. 2012. "Conformational Adaptation Drives Potent, Selective and Durable Inhibition of the Human Protein Methyltransferase DOT1L." *Chemical Biology & Drug Design* 80 (6): 971–80.

Brien, Gerard L., David Remillard, Junwei Shi, Matthew L. Hemming, Jonathon Chabon, Kieran

Wynne, Eugène T. Dillon, et al. 2018. “Targeted Degradation of BRD9 Reverses Oncogenic Gene Expression in Synovial Sarcoma.” *eLife* 7 (November). https://doi.org/10.7554/eLife.41305.

Cohen, A. A., N. Geva-Zatorsky, E. Eden, M. Frenkel-Morgenstern, I. Issaeva, A. Sigal, R. Milo, et al. 2008. “Dynamic Proteomics of Individual Cancer Cells in Response to a Drug.” *Science* 322 (5907): 1511–16.

Daigle, Scott R., Edward J. Olhava, Carly A. Therkelsen, Christina R. Majer, Christopher J. Sneeringer, Jeffrey Song, L. Danielle Johnston, et al. 2011. “Selective Killing of Mixed Lineage Leukemia Cells by a Potent Small-Molecule DOT1L Inhibitor.” *Cancer Cell* 20 (1): 53–65.

Dar, Roy D., Nina N. Hosmane, Michelle R. Arkin, Robert F. Siliciano, and Leor S. Weinberger. 2014. “Screening for Noise in Gene Expression Identifies Drug Synergies.” *Science* 344 (6190): 1392–96.

Fallahi-Sichani, Mohammad, Verena Becker, Benjamin Izar, Gregory J. Baker, Jia-Ren Lin, Sarah A. Boswell, Parin Shah, Asaf Rotem, Levi A. Garraway, and Peter K. Sorger. 2017. “Adaptive Resistance of Melanoma Cells to RAF Inhibition via Reversible Induction of a Slowly Dividing de-Differentiated State.” *Molecular Systems Biology* 13 (1): 905.

Garraway, Levi A., and Pasi A. Jänne. 2012. “Circumventing Cancer Drug Resistance in the Era of Personalized Medicine.” *Cancer Discovery*. https://doi.org/10.1158/2159-8290.cd-12-0012.

Gupta, Piyush B., Christine M. Fillmore, Guozhi Jiang, Sagi D. Shapira, Kai Tao, Charlotte Kuperwasser, and Eric S. Lander. 2011. “Stochastic State Transitions Give Rise to Phenotypic Equilibrium in Populations of Cancer Cells.” *Cell* 146 (4): 633–44.

Hartman, Mariusz L., and Malgorzata Czyz. 2015. “MITF in Melanoma: Mechanisms behind Its Expression and Activity.” *Cellular and Molecular Life Sciences: CMLS* 72 (7): 1249–60.

Harvey, Kieran F., Xiaomeng Zhang, and David M. Thomas. 2013. “The Hippo Pathway and Human Cancer.” *Nature Reviews. Cancer* 13 (4): 246–57.

Huang, Yu-Han, Olaf Klingbeil, Xue-Yan He, Xiaoli S. Wu, Gayatri Arun, Bin Lu, Tim D. D. Somerville, et al. 2018. “POU2F3 Is a Master Regulator of a Tuft Cell-like Variant of Small Cell Lung Cancer.” *Genes & Development* 32 (13-14): 915–28.

Joung, Julia, Jesse M. Engreitz, Silvana Konermann, Omar O. Abudayyeh, Vanessa K. Verdine, Francois Aguet, Jonathan S. Gootenberg, et al. 2017. “Genome-Scale Activation Screen Identifies a lncRNA Locus Regulating a Gene Neighbourhood.” *Nature* 548 (7667): 343–46.

Kitago, Minoru, Steve R. Martinez, Takeshi Nakamura, Myung-Shin Sim, and Dave S. B. Hoon. 2009. “Regulation of RUNX3 Tumor Suppressor Gene Expression in Cutaneous Melanoma.” *Clinical Cancer Research: An Official Journal of the American Association for Cancer Research* 15 (9): 2988–94.

Konermann, Silvana, Mark D. Brigham, Alexandro E. Trevino, Julia Joung, Omar O. Abudayyeh, Clea Barcena, Patrick D. Hsu, et al. 2014. “Genome-Scale Transcriptional Activation by an Engineered CRISPR-Cas9 Complex.” *Nature*, December. https://doi.org/10.1038/nature14136.

Lu, Lei, Yan Gao, Zan Zhang, Qing Cao, Xuena Zhang, Jianghuan Zou, and Ying Cao. 2015. “Kdm2a/b Lysine Demethylases Regulate Canonical Wnt Signaling by Modulating the Stability of Nuclear β-Catenin.” *Developmental Cell* 33 (6): 660–74.

Maamar, Hédia, Arjun Raj, and David Dubnau. 2007. “Noise in Gene Expression Determines Cell Fate in Bacillus Subtilis.” *Science* 317 (5837): 526–29.

Mojtahedi, Mitra, Alexander Skupin, Joseph Zhou, Ivan G. Castaño, Rebecca Y. Y. Leong-Quong, Hannah Chang, Kalliopi Trachana, Alessandro Giuliani, and Sui Huang.

2016. “Cell Fate Decision as High-Dimensional Critical State Transition.” *PLoS Biology* 14 (12): e2000640.

Okada, M., S. Nada, Y. Yamanashi, T. Yamamoto, and H. Nakagawa. 1991. “CSK: A Protein-Tyrosine Kinase Involved in Regulation of Src Family Kinases.” *The Journal of Biological Chemistry* 266 (36): 24249–52.

Pisco, A. O., and S. Huang. 2015. “Non-Genetic Cancer Cell Plasticity and Therapy-Induced Stemness in Tumour Relapse: ‘What Does Not Kill Me Strengthens Me.’” *British Journal of Cancer* 112 (11): 1725–32.

Raj, Arjun, and Alexander van Oudenaarden. 2008. “Nature, Nurture, or Chance: Stochastic Gene Expression and Its Consequences.” *Cell* 135 (2): 216–26.

Raj, Arjun, Scott A. Rifkin, Erik Andersen, and Alexander van Oudenaarden. 2010. “Variability in Gene Expression Underlies Incomplete Penetrance.” *Nature* 463 (7283): 913–18.

Rambow, Florian, Aljosja Rogiers, Oskar Marin-Bejar, Sara Aibar, Julia Femel, Michael Dewaele, Panagiotis Karras, et al. 2018. “Toward Minimal Residual Disease-Directed Therapy in Melanoma.” *Cell* 0 (0). https://doi.org/10.1016/j.cell.2018.06.025.

Segura, Miguel F., Bárbara Fontanals-Cirera, Avital Gaziel-Sovran, María V. Guijarro, Doug Hanniford, Guangtao Zhang, Pilar González-Gomez, et al. 2013. “BRD4 Sustains Melanoma Proliferation and Represents a New Target for Epigenetic Therapy.” *Cancer Research* 73 (20): 6264–76.

Shaffer, Sydney M., Margaret C. Dunagin, Stefan R. Torborg, Eduardo A. Torre, Benjamin Emert, Clemens Krepler, Marilda Beqiri, et al. 2017. “Rare Cell Variability and Drug-Induced Reprogramming as a Mode of Cancer Drug Resistance.” *Nature* 546 (7658): 431–35.

Shaffer, Sydney M., Benjamin L. Emert, Ann E. Sizemore, Rohit Gupte, Eduardo Torre, Danielle S. Bassett, and Arjun Raj. 2018. “Memory Sequencing Reveals Heritable Single Cell Gene Expression Programs Associated with Distinct Cellular Behaviors.” *bioRxiv*. https://doi.org/10.1101/379016.

Shalem, Ophir, Neville E. Sanjana, Ella Hartenian, Xi Shi, David A. Scott, Tarjei S. Mikkelsen, Dirk Heckl, et al. 2014. “Genome-Scale CRISPR-Cas9 Knockout Screening in Human Cells.” *Science* 343 (6166): 84–87.

Sharma, Sreenath V., Diana Y. Lee, Bihua Li, Margaret P. Quinlan, Fumiyuki Takahashi, Shyamala Maheswaran, Ultan McDermott, et al. 2010. “A Chromatin-Mediated Reversible Drug-Tolerant State in Cancer Cell Subpopulations.” *Cell* 141 (1): 69–80.

Shi, Junwei, Eric Wang, Joseph P. Milazzo, Zihua Wang, Justin B. Kinney, and Christopher R. Vakoc. 2015. “Discovery of Cancer Drug Targets by CRISPR-Cas9 Screening of Protein Domains.” *Nature Biotechnology* 33 (6): 661–67.

Strub, Thomas, Flavia G. Ghiraldini, Saul Carcamo, Man Li, Aleksandra Wroblewska, Rajendra Singh, Matthew S. Goldberg, et al. 2018. “SIRT6 Haploinsufficiency Induces BRAFV600E Melanoma Cell Resistance to MAPK Inhibitors via IGF Signalling.” *Nature Communications* 9 (1): 3440.

Subramanian, Aravind, Pablo Tamayo, Vamsi K. Mootha, Sayan Mukherjee, Benjamin L. Ebert, Michael A. Gillette, Amanda Paulovich, et al. 2005. “Gene Set Enrichment Analysis: A Knowledge-Based Approach for Interpreting Genome-Wide Expression Profiles.” *Proceedings of the National Academy of Sciences of the United States of America* 102 (43): 15545–50.

Süel, Gürol M., Rajan P. Kulkarni, Jonathan Dworkin, Jordi Garcia-Ojalvo, and Michael B. Elowitz. 2007. “Tunability and Noise Dependence in Differentiation Dynamics.” *Science* 315 (5819): 1716–19.

Sun, Chong, Liqin Wang, Sidong Huang, Guus J. J. E. Heynen, Anirudh Prahallad, Caroline

Robert, John Haanen, et al. 2014. “Reversible and Adaptive Resistance to BRAF(V600E) Inhibition in Melanoma.” *Nature* 508 (7494): 118–22.

Su, Yapeng, Wei Wei, Lidia Robert, Min Xue, Jennifer Tsoi, Angel Garcia-Diaz, Blanca Homet Moreno, et al. 2017. “Single-Cell Analysis Resolves the Cell State Transition and Signaling Dynamics Associated with Melanoma Drug-Induced Resistance.” *Proceedings of the National Academy of Sciences of the United States of America* 114 (52): 13679–84.

Symmons, Orsolya, and Arjun Raj. 2016. “What’s Luck Got to Do with It: Single Cells, Multiple Fates, and Biological Nondeterminism.” *Molecular Cell* 62 (5): 788–802.

Tarumoto, Yusuke, Bin Lu, Tim D. D. Somerville, Yu-Han Huang, Joseph P. Milazzo, Xiaoli S. Wu, Olaf Klingbeil, Osama El Demerdash, Junwei Shi, and Christopher R. Vakoc. 2018. “LKB1, Salt-Inducible Kinases, and MEF2C Are Linked Dependencies in Acute Myeloid Leukemia.” *Molecular Cell* 69 (6): 1017–27.e6.

Tirosh, Itay, Benjamin Izar, Sanjay M. Prakadan, Marc H. Wadsworth 2nd, Daniel Treacy, John J. Trombetta, Asaf Rotem, et al. 2016. “Dissecting the Multicellular Ecosystem of Metastatic Melanoma by Single-Cell RNA-Seq.” *Science* 352 (6282): 189–96.

Torre, Eduardo, Hannah Dueck, Sydney Shaffer, Janko Gospocic, Rohit Gupte, Roberto Bonasio, Junhyong Kim, John Murray, and Arjun Raj. 2018. “Rare Cell Detection by Single-Cell RNA Sequencing as Guided by Single-Molecule RNA FISH.” *Cell Systems*, February. https://doi.org/10.1016/j.cels.2018.01.014.

Trunzer, Kerstin, Anna C. Pavlick, Lynn Schuchter, Rene Gonzalez, Grant A. McArthur, Thomas E. Hutson, Stergios J. Moschos, et al. 2013. “Pharmacodynamic Effects and Mechanisms of Resistance to Vemurafenib in Patients with Metastatic Melanoma.” *Journal of Clinical Oncology: Official Journal of the American Society of Clinical Oncology* 31 (14): 1767–74.

Weinreb, Caleb, Alejo E. Rodriguez-Fraticelli, Fernando D. Camargo, and Allon M. Klein. 2018. “Lineage Tracing on Transcriptional Landscapes Links State to Fate during Differentiation.” *bioRxiv*. https://doi.org/10.1101/467886.

Wellbrock, Claudia, and Imanol Arozarena. 2015. “Microphthalmia-Associated Transcription Factor in Melanoma Development and MAP-Kinase Pathway Targeted Therapy.” *Pigment Cell & Melanoma Research* 28 (4): 390–406.

Wernet, Mathias F., Esteban O. Mazzoni, Arzu Celik, Dianne M. Duncan, Ian Duncan, and Claude Desplan. 2006. “Stochastic Spineless Expression Creates the Retinal Mosaic for Colour Vision.” *Nature* 440 (7081): 174–80.

Zhu, Bo, Shuyang Chen, Hongshen Wang, Chengqian Yin, Changpeng Han, Cong Peng, Zhaoqian Liu, et al. 2018. “The Protective Role of DOT1L in UV-Induced Melanomagenesis.” *Nature Communications* 9 (1): 259.

Figure 1

A The fate of a cell depends on its molecular state at the time of drug exposure

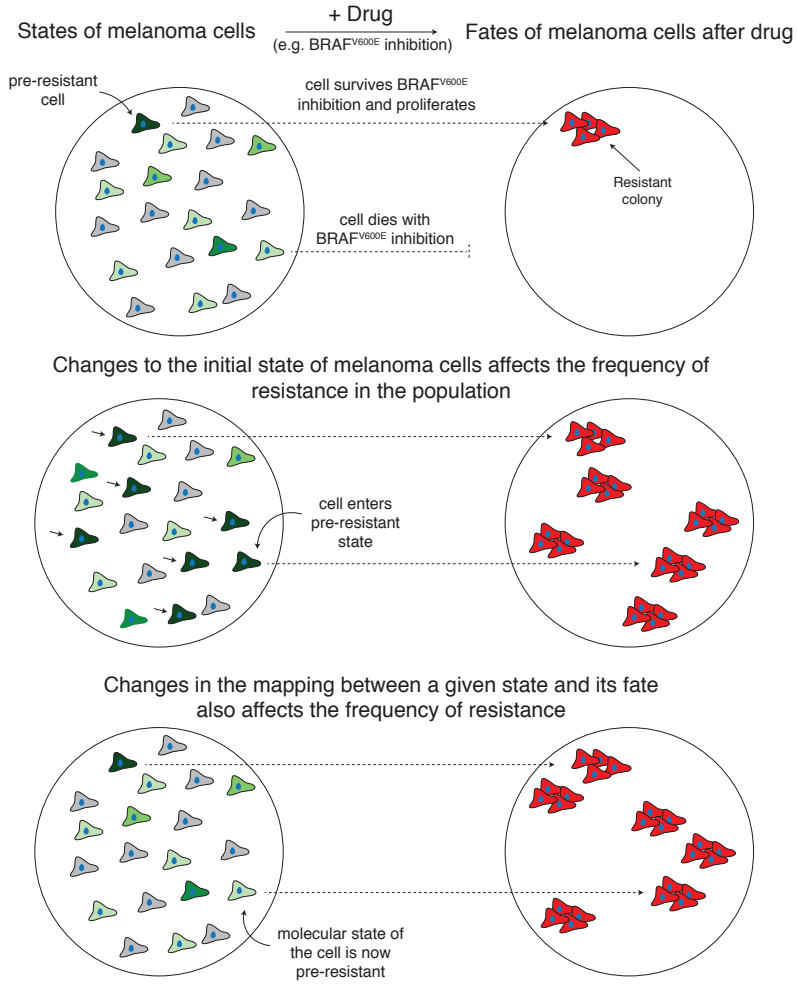

B Pooled CRISPR screening scheme for modulators of cellular state

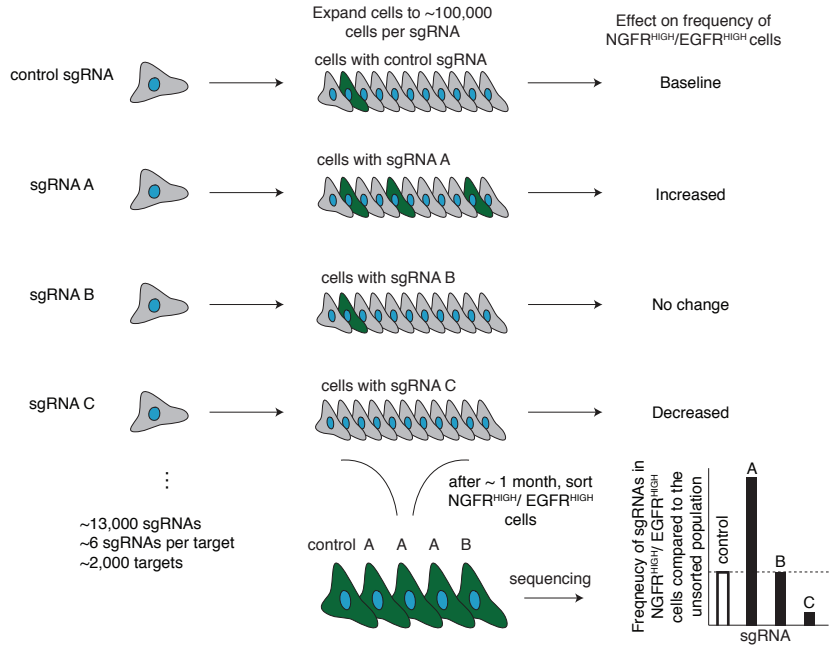

Figure 2

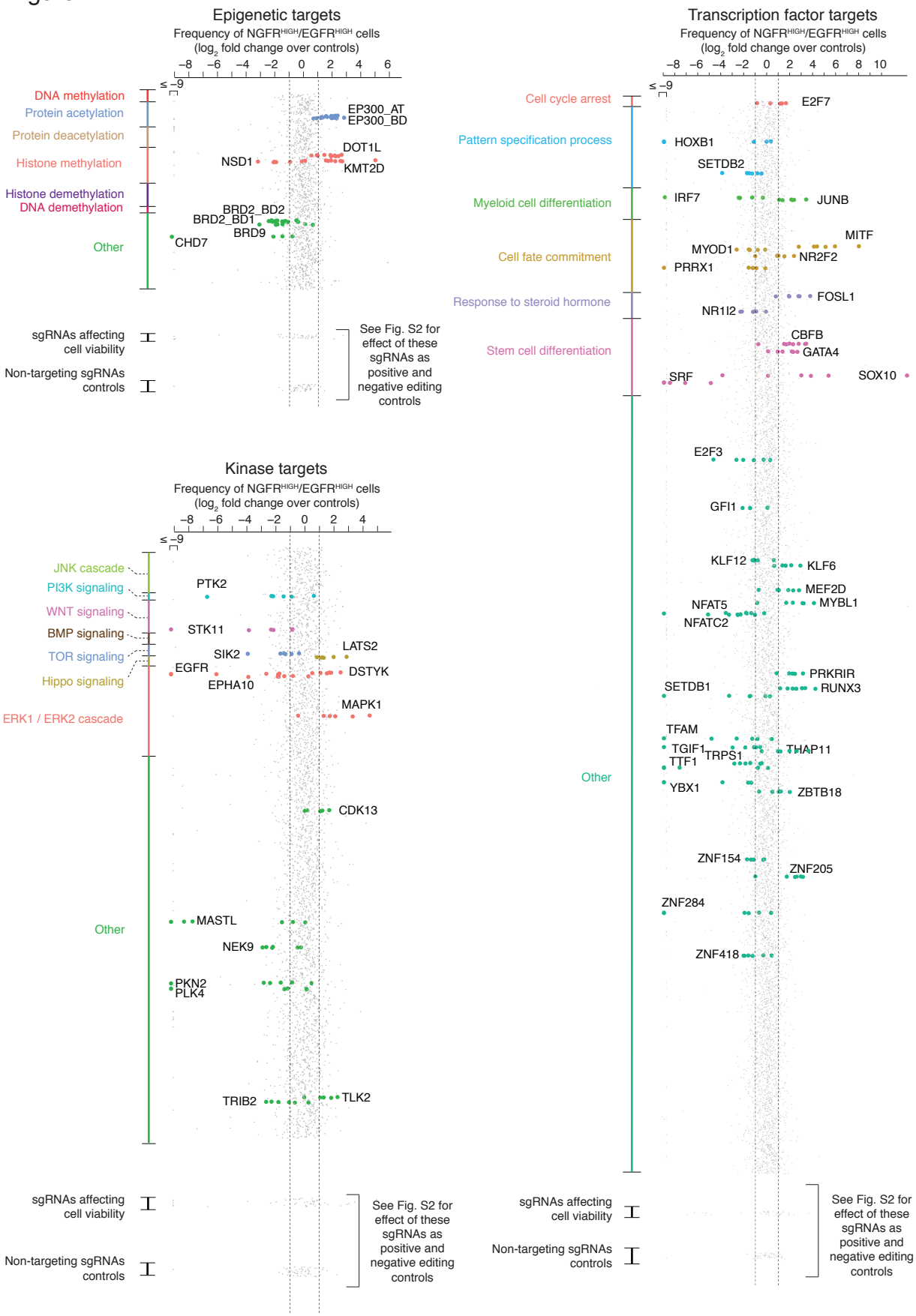
Epigenetic targets
Frequency of NGFR^HIGH/EGFR^HIGH cells
(log2 fold change over controls)
−8 −6 −4 −2 0 2 4 6
≤ −9
DNA methylation
Protein acetylation
Protein deacetylation
Histone methylation
Histone demethylation
DNA demethylation
Other
EP300_AT
EP300_BD
DOT1L
NSD1
KMT2D
BRD2_BD2
BRD2_BD1
BRD9
CHD7
sgRNAs affecting cell viability
Non-targeting sgRNAs controls
See Fig. S2 for effect of these sgRNAs as positive and negative editing controls
Transcription factor targets
Frequency of NGFR^HIGH/EGFR^HIGH cells
(log2 fold change over controls)
−8 −6 −4 −2 0 2 4 6 8 10
≤ −9
Cell cycle arrest
Pattern specification process
Myeloid cell differentiation
Cell fate commitment
Response to steroid hormone
Stem cell differentiation
Other
E2F7
HOXB1
SETDB2
IRF7
JUNB
MITF
MYOD1
NR2F2
PRRX1
FOSL1
NR1I2
CBFB
GATA4
SRF
SOX10
E2F3
GFI1
KLF12
KLF6
MEF2D
MYBL1
NFAT5
NFATC2
PRKRIR
SETDB1
RUNX3
TFAM
TGIF1
TRPS1
THAP11
TTF1
YBX1
ZBTB18
ZNF154
ZNF205
ZNF284
ZNF418
sgRNAs affecting cell viability
Non-targeting sgRNAs controls
See Fig. S2 for effect of these sgRNAs as positive and negative editing controls
Kinase targets
Frequency of NGFR^HIGH/EGFR^HIGH cells
(log2 fold change over controls)
−8 −6 −4 −2 0 2 4
≤ −9
JNK cascade
PI3K signaling
WNT signaling
BMP signaling
TOR signaling
Hippo signaling
ERK1 / ERK2 cascade
Other
PTK2
STK11
LATS2
SIK2
EGFR
DSTYK
EPHA10
MAPK1
CDK13
MASTL
NEK9
PKN2
PLK4
TRIB2
TLK2
sgRNAs affecting cell viability
Non-targeting sgRNAs controls
See Fig. S2 for effect of these sgRNAs as positive and negative editing controls

Figure 3

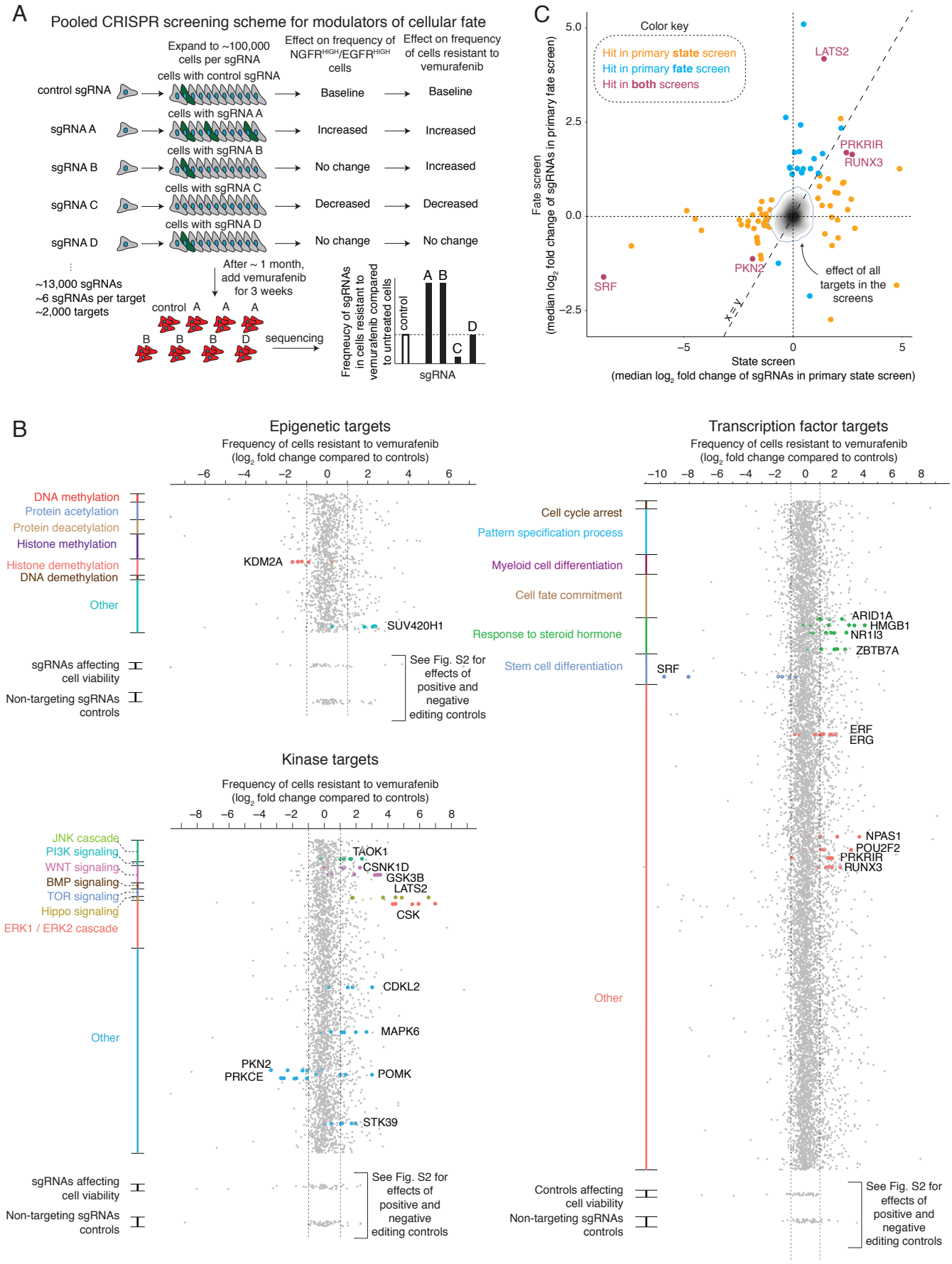
A
Pooled CRISPR screening scheme for modulators of cellular fate
Expand to ~100,000 cells per sgRNA
Effect on frequency of NGFR^HIGH/EGFR^HIGH cells
Effect on frequency of cells resistant to vemurafenib
control sgRNA
cells with control sgRNA
Baseline
Baseline
sgRNA A
cells with sgRNA A
Increased
Increased
sgRNA B
cells with sgRNA B
No change
Increased
sgRNA C
cells with sgRNA C
Decreased
Decreased
sgRNA D
cells with sgRNA D
No change
No change
~13,000 sgRNAs
~6 sgRNAs per target
~2,000 targets
After ~ 1 month, add vemurafenib for 3 weeks
control
sequencing
Frequency of sgRNAs in cells resistant to vemurafenib compared to untreated cells
sgRNA
C
Color key
Hit in primary state screen
Hit in primary fate screen
Hit in both screens
LATS2
PRKRIR
RUNX3
PKN2
SRF
effect of all targets in the screens
Fate screen (median log2 fold change of sgRNAs in primary fate screen)
State screen (median log2 fold change of sgRNAs in primary state screen)
B
Epigenetic targets
Frequency of cells resistant to vemurafenib (log2 fold change compared to controls)
DNA methylation
Protein acetylation
Protein deacetylation
Histone methylation
Histone demethylation
DNA demethylation
Other
KDM2A
SUV420H1
sgRNAs affecting cell viability
Non-targeting sgRNAs controls
See Fig. S2 for effects of positive and negative editing controls
Kinase targets
Frequency of cells resistant to vemurafenib (log2 fold change compared to controls)
JNK cascade
PI3K signaling
WNT signaling
BMP signaling
TOR signaling
Hippo signaling
ERK1 / ERK2 cascade
Other
TAOK1
CSNK1D
GSK3B
LATS2
CSK
CDKL2
MAPK6
PKN2
PRKCE
POMK
STK39
sgRNAs affecting cell viability
Non-targeting sgRNAs controls
See Fig. S2 for effects of positive and negative editing controls
Transcription factor targets
Frequency of cells resistant to vemurafenib (log2 fold change compared to controls)
Cell cycle arrest
Pattern specification process
Myeloid cell differentiation
Cell fate commitment
Response to steroid hormone
Stem cell differentiation
Other
ARID1A
HMGB1
NR1I3
ZBTB7A
SRF
ERF
ERG
NPAS1
POU2F2
PRKRIR
RUNX3
Controls affecting cell viability
Non-targeting sgRNAs controls
See Fig. S2 for effects of positive and negative editing controls

Figure 4

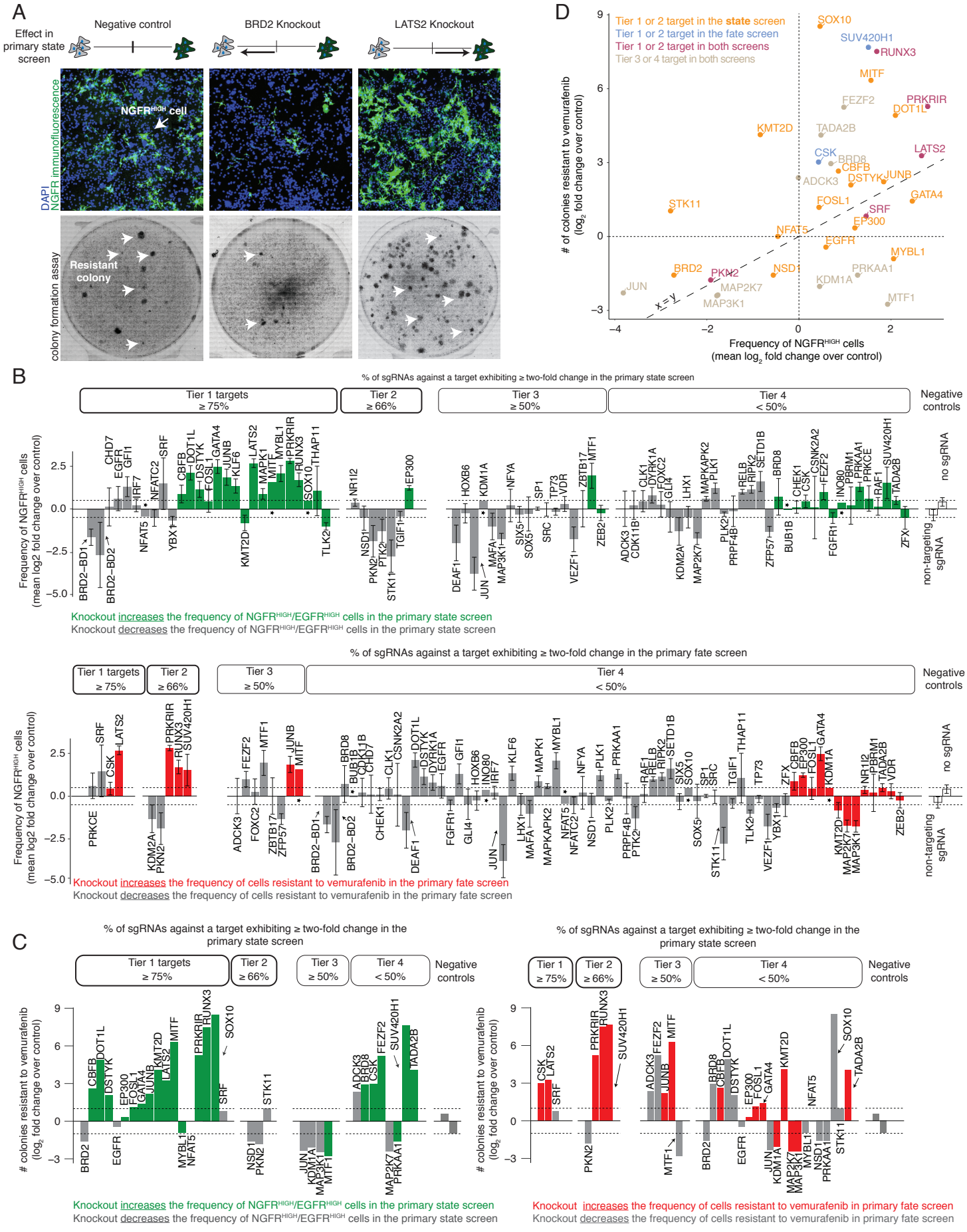
A
Negative control
BRD2 Knockout
LATS2 Knockout
Effect in primary state screen
DAPI
NGFR immunofluorescence
NGFR^HIGH cell
colony formation assay
Resistant colony
D
Tier 1 or 2 target in the state screen
Tier 1 or 2 target in the fate screen
Tier 1 or 2 target in both screens
Tier 3 or 4 target in both screens
# of colonies resistant to vemurafenib (log2 fold change over control)
Frequency of NGFR^HIGH cells (mean log2 fold change over control)
x = y
B
% of sgRNAs against a target exhibiting ≥ two-fold change in the primary state screen
Tier 1 targets ≥ 75%
Tier 2 ≥ 66%
Tier 3 ≥ 50%
Tier 4 < 50%
Negative controls
Frequency of NGFR^HIGH cells (mean log2 fold change over control)
no sgRNA
non-targeting sgRNA
Knockout increases the frequency of NGFR^HIGH/EGFR^HIGH cells in the primary state screen
Knockout decreases the frequency of NGFR^HIGH/EGFR^HIGH cells in the primary state screen
% of sgRNAs against a target exhibiting ≥ two-fold change in the primary fate screen
Knockout increases the frequency of cells resistant to vemurafenib in the primary fate screen
Knockout decreases the frequency of cells resistant to vemurafenib in the primary fate screen
C
% of sgRNAs against a target exhibiting ≥ two-fold change in the primary state screen
# colonies resistant to vemurafenib (log2 fold change over control)
Knockout increases the frequency of NGFR^HIGH/EGFR^HIGH cells in the primary state screen
Knockout decreases the frequency of NGFR^HIGH/EGFR^HIGH cells in the primary state screen
Knockout increases the frequency of cells resistant to vemurafenib in primary fate screen
Knockout decreases the frequency of cells resistant to vemurafenib in primary fate screen

Figure 5

A

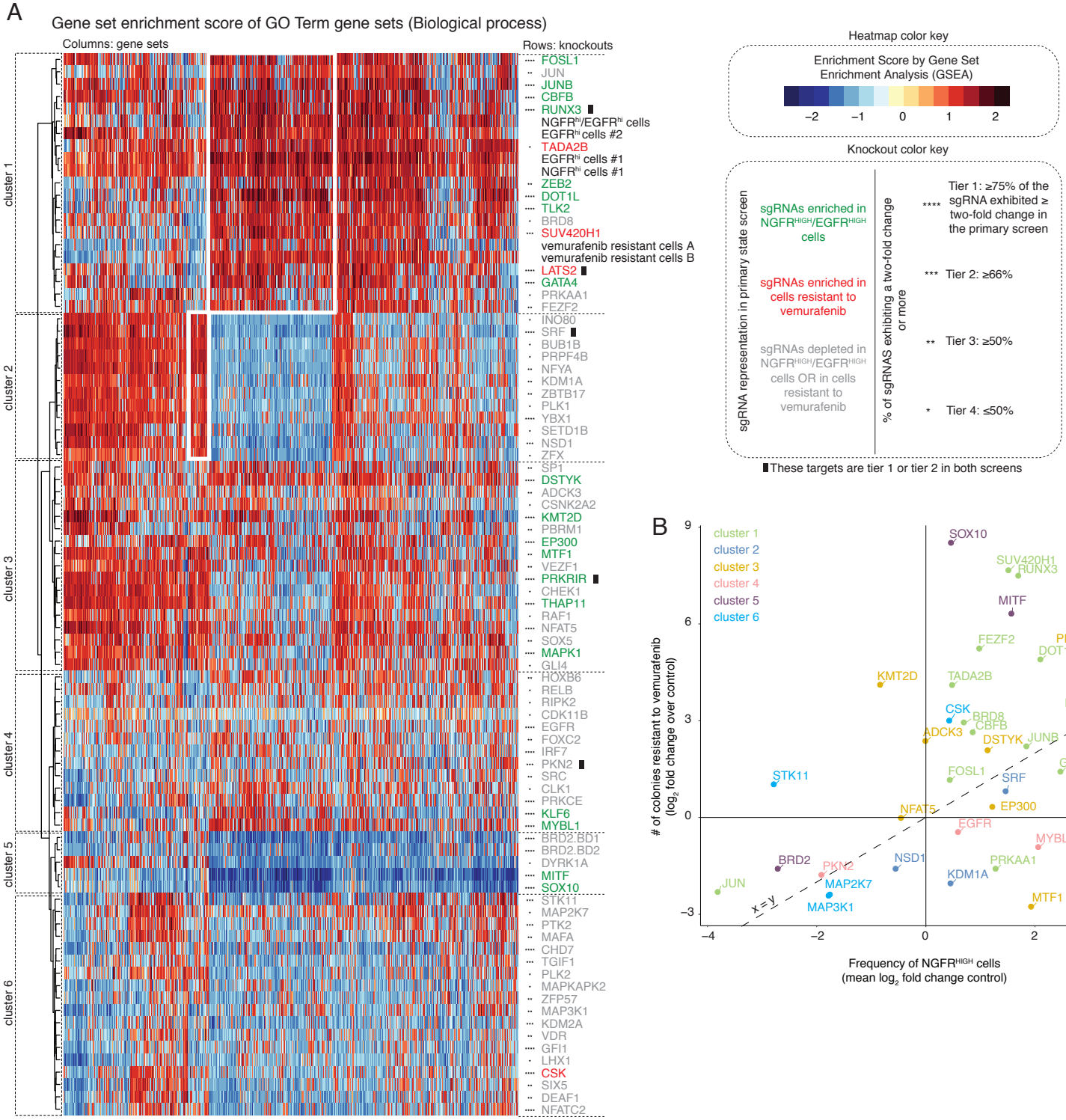
Gene set enrichment score of GO Term gene sets (Biological process)
Columns: gene sets
Rows: knockouts
cluster 1
cluster 2
cluster 3
cluster 4
cluster 5
cluster 6
FOSL1
JUN
JUNB
CBFB
RUNX3
NGFRhi/EGFRhi cells
EGFRhi cells #2
TADA2B
EGFRhi cells #1
NGFRhi cells #1
ZEB2
DOT1L
TLK2
BRD8
SUV420H1
vemurafenib resistant cells A
vemurafenib resistant cells B
LATS2
GATA4
PRKAA1
FEZF2
INO80
SRF
BUB1B
PRPF4B
NFYA
KDM1A
ZBTB17
PLK1
YBX1
SETD1B
NSD1
ZFX
SP1
DSTYK
ADCK3
CSNK2A2
KMT2D
PBRM1
EP300
MTF1
VEZF1
PRKRIR
CHEK1
THAP11
RAF1
NFAT5
SOX5
MAPK1
GLI4
HOXB6
RELB
RIPK2
CDK11B
EGFR
FOXC2
IRF7
PKN2
SRC
CLK1
PRKCE
KLF6
MYBL1
BRD2.BD1
BRD2.BD2
DYRK1A
MITF
SOX10
STK11
MAP2K7
PTK2
MAFA
CHD7
TGIF1
PLK2
MAPKAPK2
ZFP57
MAP3K1
KDM2A
VDR
GFI1
LHX1
CSK
SIX5
DEAF1
NFATC2
Heatmap color key
Enrichment Score by Gene Set Enrichment Analysis (GSEA)
−2
−1
0
1
2
Knockout color key
sgRNA representation in primary state screen
sgRNAs enriched in NGFRHIGH/EGFRHIGH cells
sgRNAs enriched in cells resistant to vemurafenib
sgRNAs depleted in NGFRHIGH/EGFRHIGH cells OR in cells resistant to vemurafenib
% of sgRNAS exhibiting a two-fold change or more
**** Tier 1: ≥75% of the sgRNA exhibited ≥ two-fold change in the primary screen
*** Tier 2: ≥66%
** Tier 3: ≥50%
* Tier 4: ≤50%
These targets are tier 1 or tier 2 in both screens

B

cluster 1
cluster 2
cluster 3
cluster 4
cluster 5
cluster 6
# of colonies resistant to vemurafenib (log2 fold change over control)
Frequency of NGFRHIGH cells (mean log2 fold change control)
x = y
SOX10
SUV420H1
RUNX3
MITF
FEZF2
PRKRIR
DOT1L
KMT2D
TADA2B
LATS2
CSK
BRD8
CBFB
ADCK3
DSTYK
JUNB
GATA4
STK11
FOSL1
SRF
NFAT5
EP300
EGFR
MYBL1
BRD2
PKN2
NSD1
PRKAA1
KDM1A
JUN
MAP2K7
MAP3K1
MTF1

Figure 6

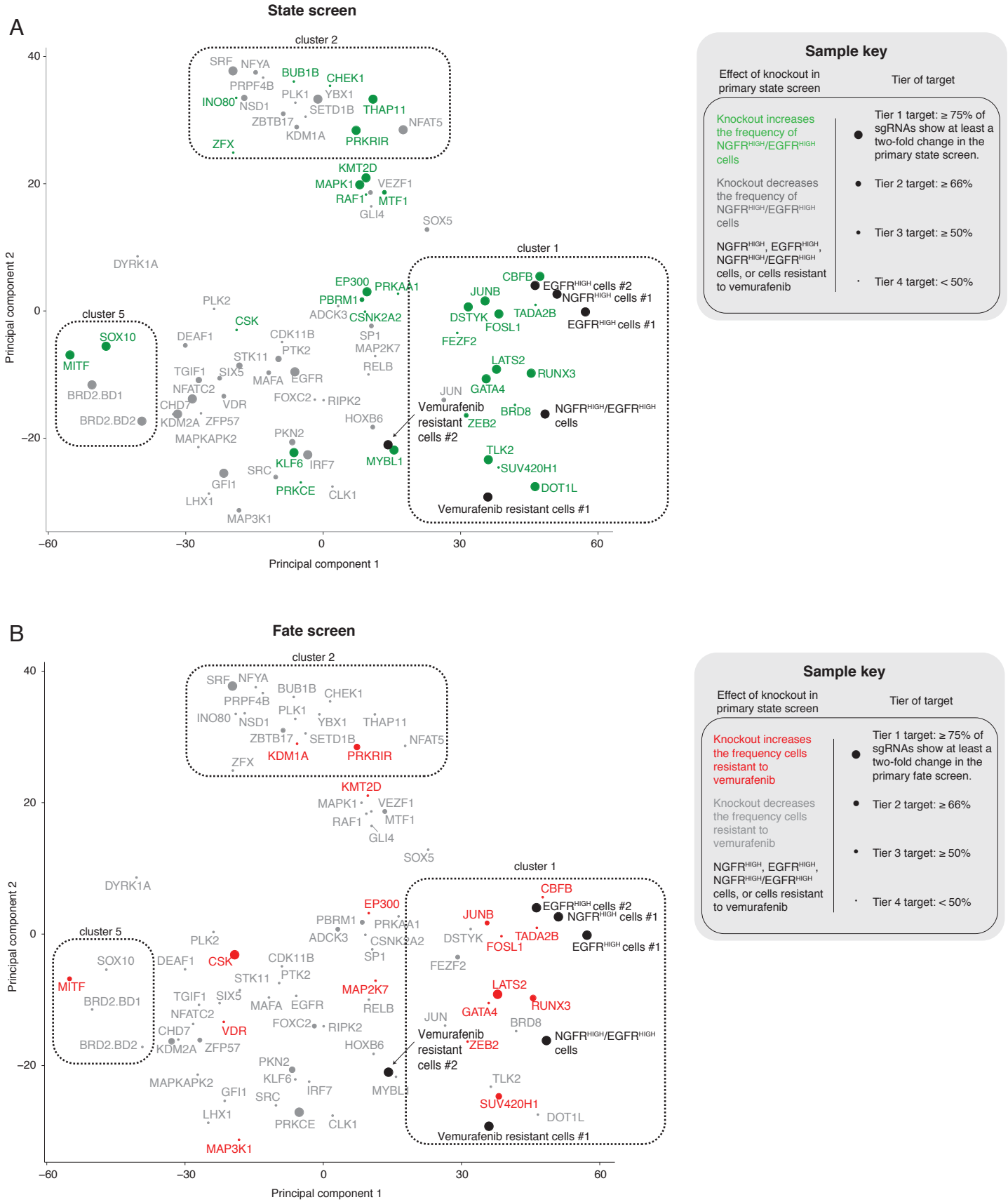
A
State screen
cluster 2
SRF
NFYA
BUB1B
CHEK1
PRPF4B
PLK1
YBX1
INO80
NSD1
SETD1B
THAP11
ZBTB17
NFAT5
KDM1A
PRKRIR
ZFX
KMT2D
MAPK1
VEZF1
RAF1
MTF1
GLI4
SOX5
DYRK1A
cluster 1
CBFB
EGFR^HIGH cells #2
NGFR^HIGH cells #1
EP300
PRKAA1
JUNB
PLK2
PBRM1
ADCK3
CSNK2A2
DSTYK
TADA2B
FOSL1
EGFR^HIGH cells #1
cluster 5
CSK
SOX10
DEAF1
CDK11B
SP1
FEZF2
PTK2
MAP2K7
MITF
STK11
RELB
LATS2
TGIF1
SIX5
RUNX3
MAFA
EGFR
GATA4
BRD2.BD1
NFATC2
JUN
CHD7
VDR
FOXC2
RIPK2
BRD8
NGFR^HIGH/EGFR^HIGH cells
BRD2.BD2
KDM2A
ZFP57
HOXB6
Vemurafenib resistant cells #2
ZEB2
MAPKAPK2
PKN2
TLK2
KLF6
IRF7
MYBL1
SUV420H1
SRC
GFI1
DOT1L
PRKCE
CLK1
LHX1
Vemurafenib resistant cells #1
MAP3K1
Principal component 2
Principal component 1
40
20
0
−20
−60
−30
0
30
60
Sample key
Effect of knockout in primary state screen
Tier of target
Knockout increases the frequency of NGFR^HIGH/EGFR^HIGH cells
Knockout decreases the frequency of NGFR^HIGH/EGFR^HIGH cells
NGFR^HIGH, EGFR^HIGH, NGFR^HIGH/EGFR^HIGH cells, or cells resistant to vemurafenib
Tier 1 target: ≥ 75% of sgRNAs show at least a two-fold change in the primary state screen.
Tier 2 target: ≥ 66%
Tier 3 target: ≥ 50%
Tier 4 target: < 50%
B
Fate screen
cluster 2
SRF
NFYA
BUB1B
CHEK1
PRPF4B
PLK1
INO80
NSD1
YBX1
THAP11
ZBTB17
SETD1B
NFAT5
ZFX
KDM1A
PRKRIR
KMT2D
MAPK1
VEZF1
RAF1
MTF1
GLI4
SOX5
DYRK1A
cluster 1
CBFB
EGFR^HIGH cells #2
NGFR^HIGH cells #1
EP300
PRKAA1
JUNB
PBRM1
ADCK3
CSNK2A2
DSTYK
TADA2B
FOSL1
EGFR^HIGH cells #1
cluster 5
PLK2
CSK
SOX10
DEAF1
CDK11B
SP1
FEZF2
PTK2
MITF
STK11
MAP2K7
LATS2
BRD2.BD1
TGIF1
SIX5
RUNX3
MAFA
EGFR
RELB
GATA4
NFATC2
JUN
BRD8
CHD7
VDR
FOXC2
RIPK2
NGFR^HIGH/EGFR^HIGH cells
BRD2.BD2
KDM2A
ZFP57
HOXB6
Vemurafenib resistant cells #2
ZEB2
PKN2
MAPKAPK2
TLK2
KLF6
IRF7
MYBL1
GFI1
SRC
SUV420H1
DOT1L
LHX1
PRKCE
CLK1
Vemurafenib resistant cells #1
MAP3K1
Principal component 2
Principal component 1
40
20
0
−20
−60
−30
0
30
60
Sample key
Effect of knockout in primary state screen
Tier of target
Knockout increases the frequency cells resistant to vemurafenib
Knockout decreases the frequency cells resistant to vemurafenib
NGFR^HIGH, EGFR^HIGH, NGFR^HIGH/EGFR^HIGH cells, or cells resistant to vemurafenib
Tier 1 target: ≥ 75% of sgRNAs show at least a two-fold change in the primary fate screen.
Tier 2 target: ≥ 66%
Tier 3 target: ≥ 50%
Tier 4 target: < 50%

Figure 7

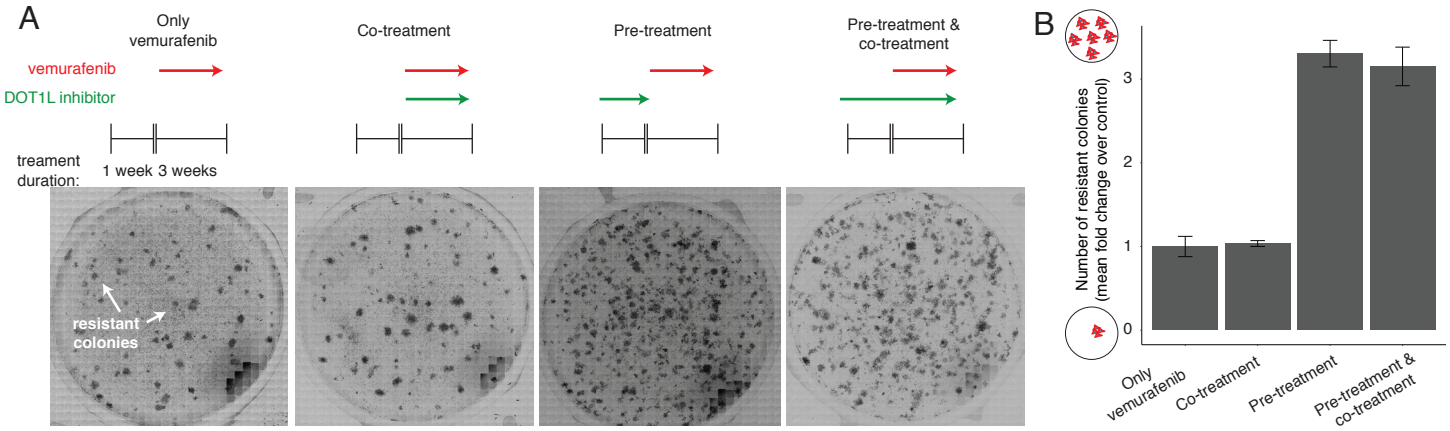
A
Only vemurafenib
Co-treatment
Pre-treatment
Pre-treatment & co-treatment
vemurafenib
DOT1L inhibitor
treament duration:
1 week 3 weeks
resistant colonies
B
Number of resistant colonies (mean fold change over control)
0
1
2
3
Only vemurafenib
Co-treatment
Pre-treatment
Pre-treatment & co-treatment

Supplemental figure 1

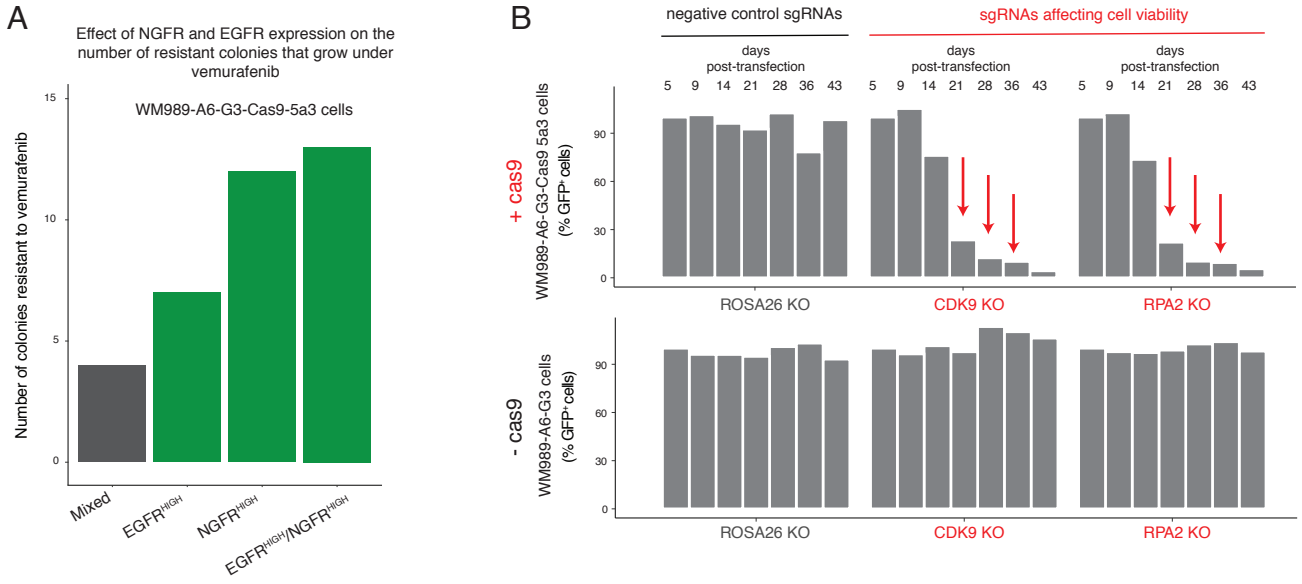

Supplemental figure 2

A Change in sgRNA representation of negative and positive controls.

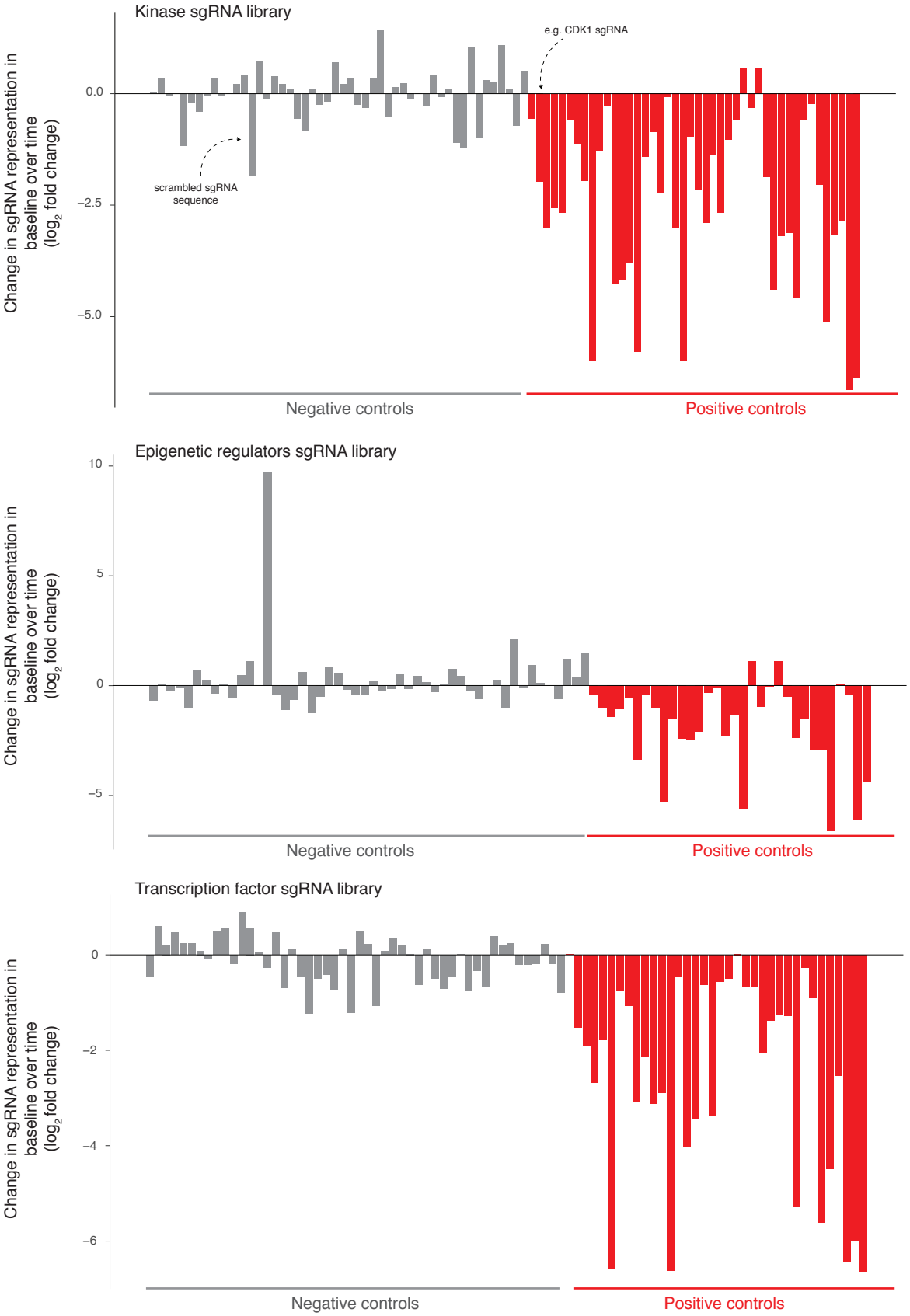

Supplemental figure 3

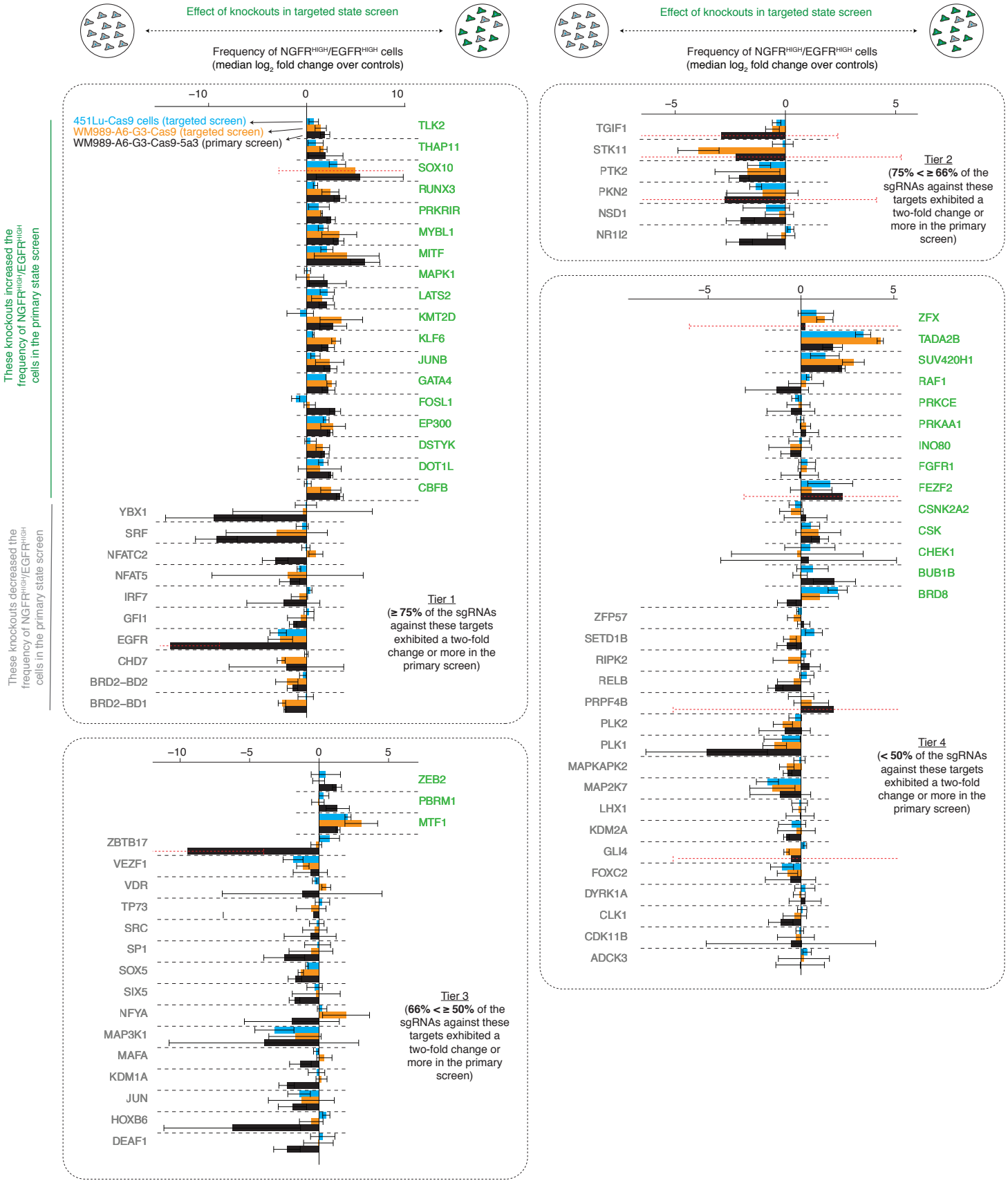

Supplemental figure 4

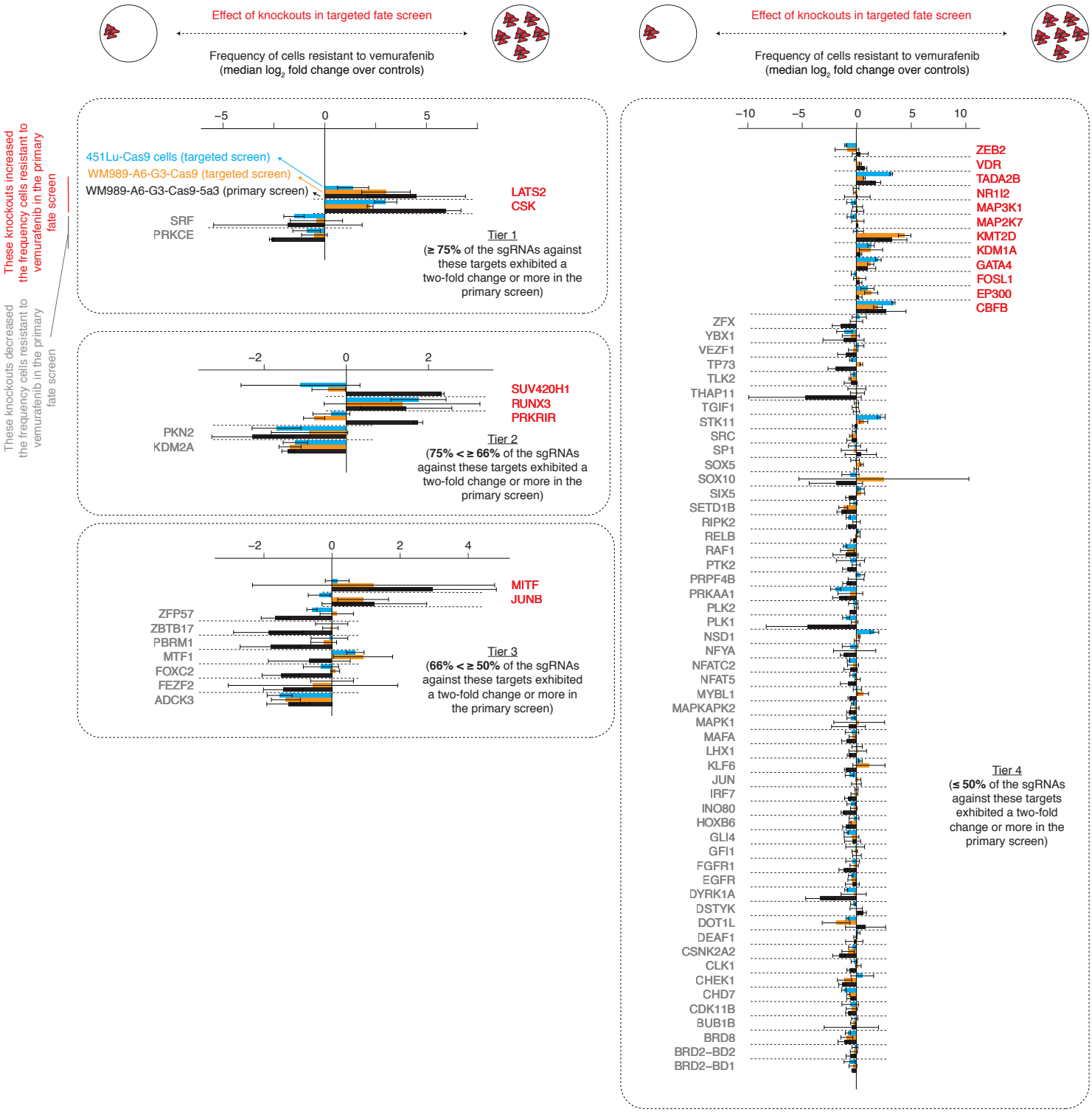

Supplemental figure 5

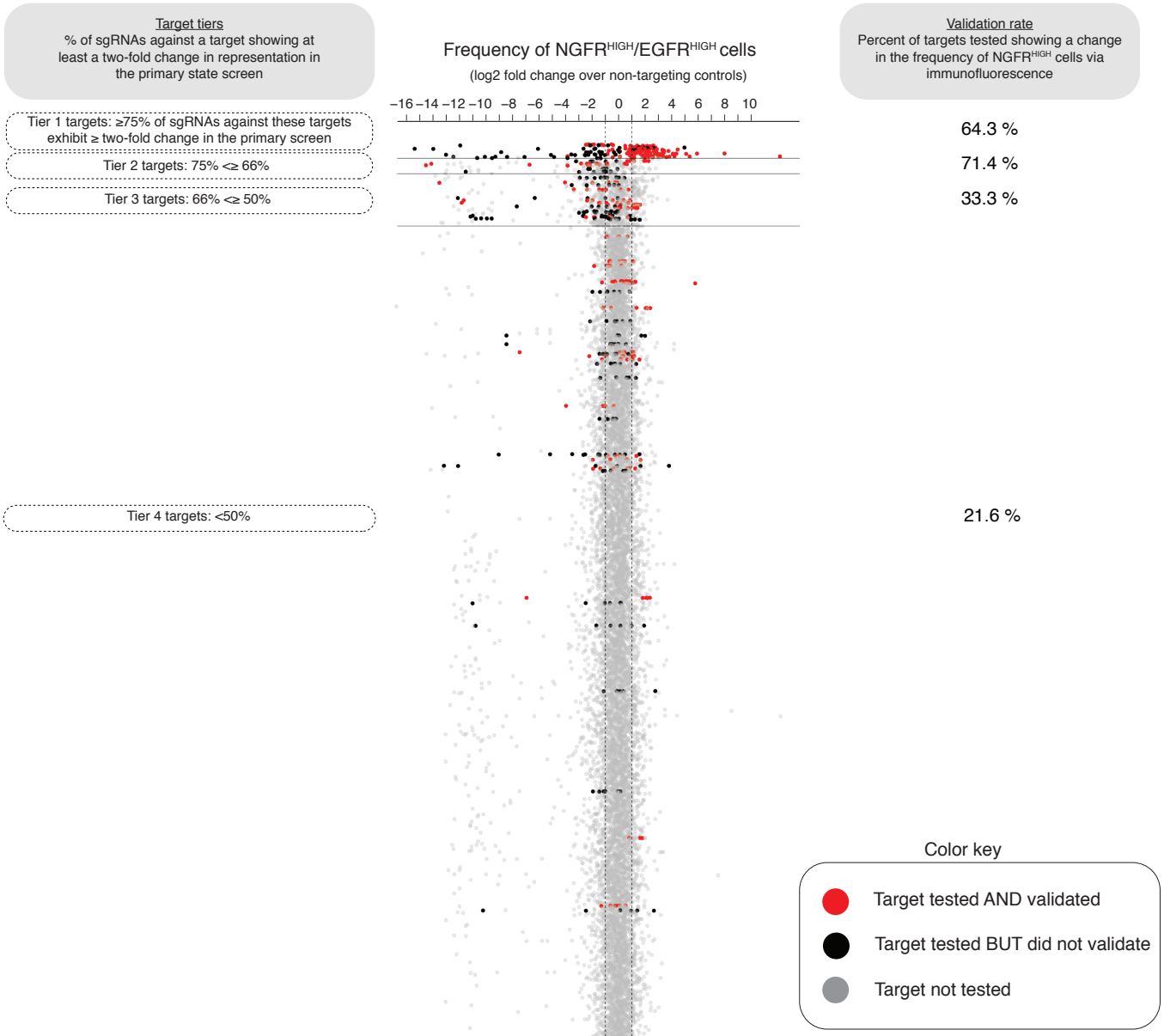

Supplemental figure 6

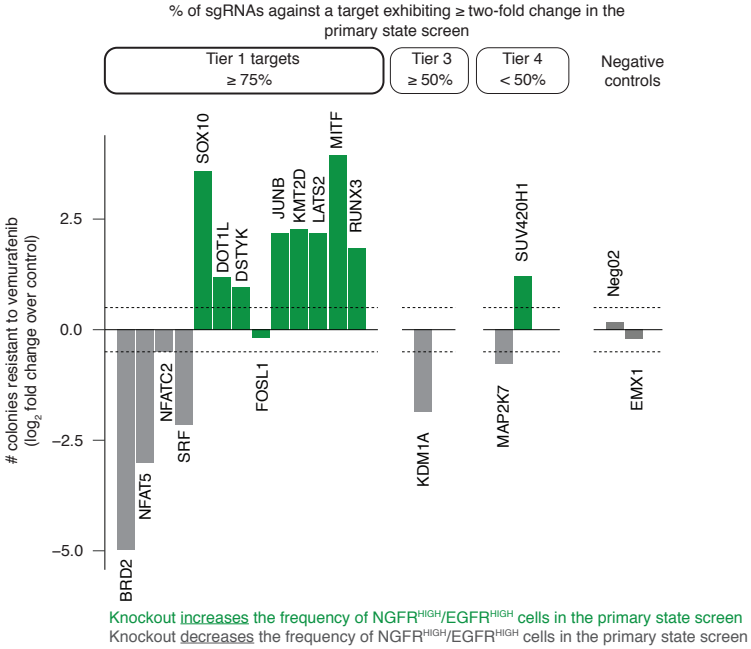

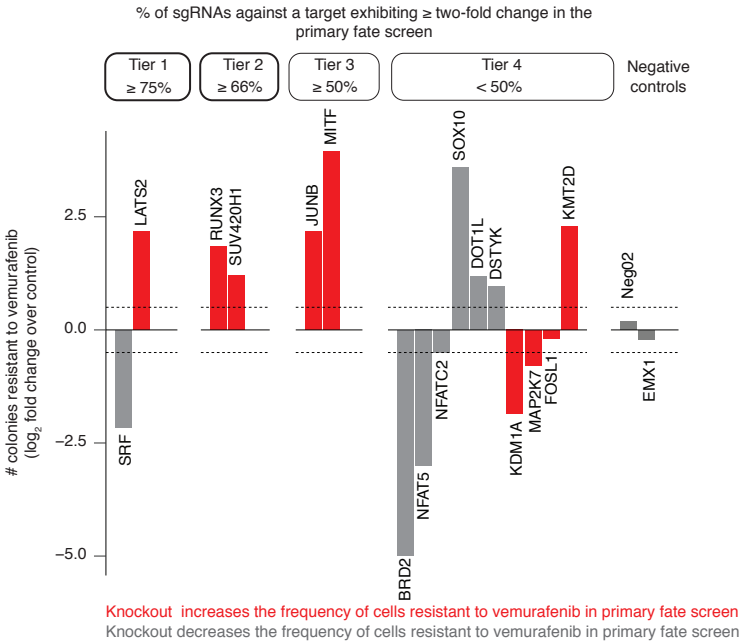

Supplemental figure 7

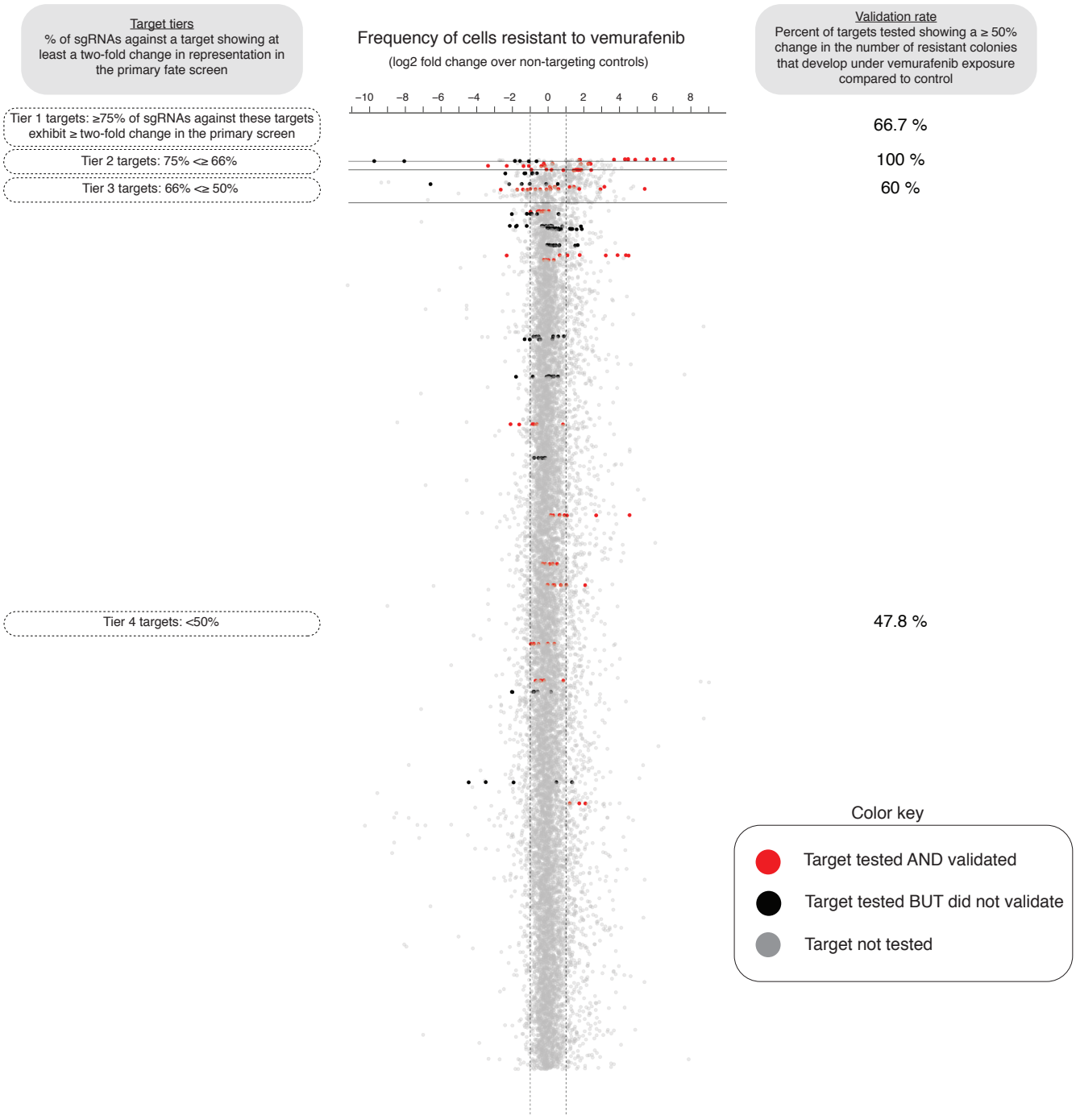

Supplemental figure 8

A

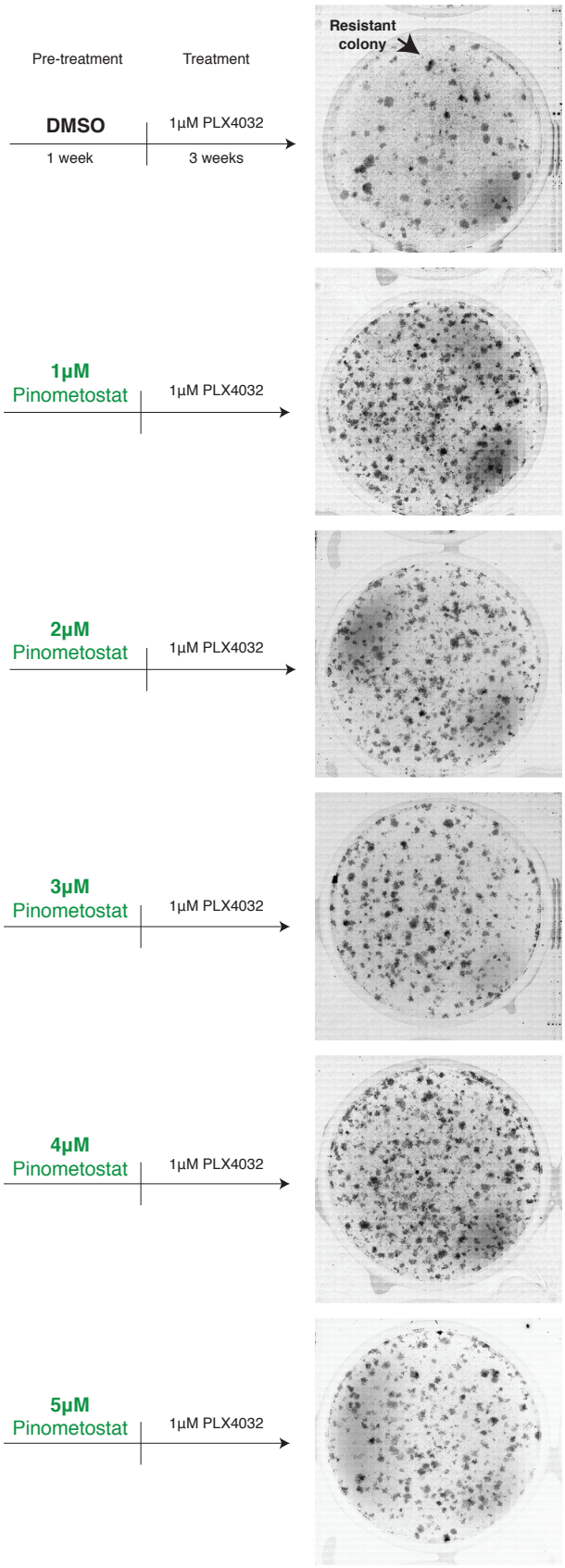

B

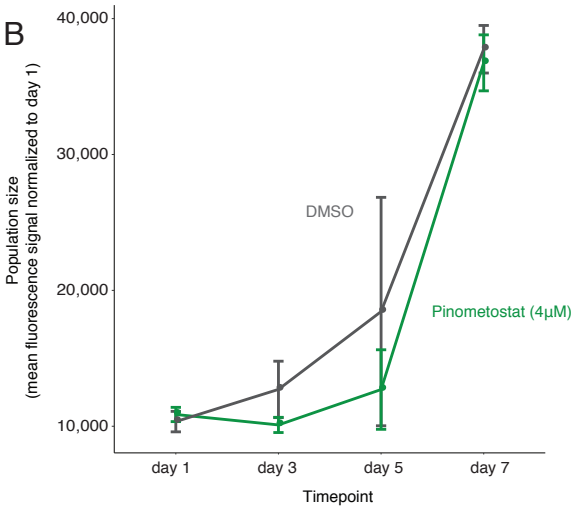

Supplemental figure 9

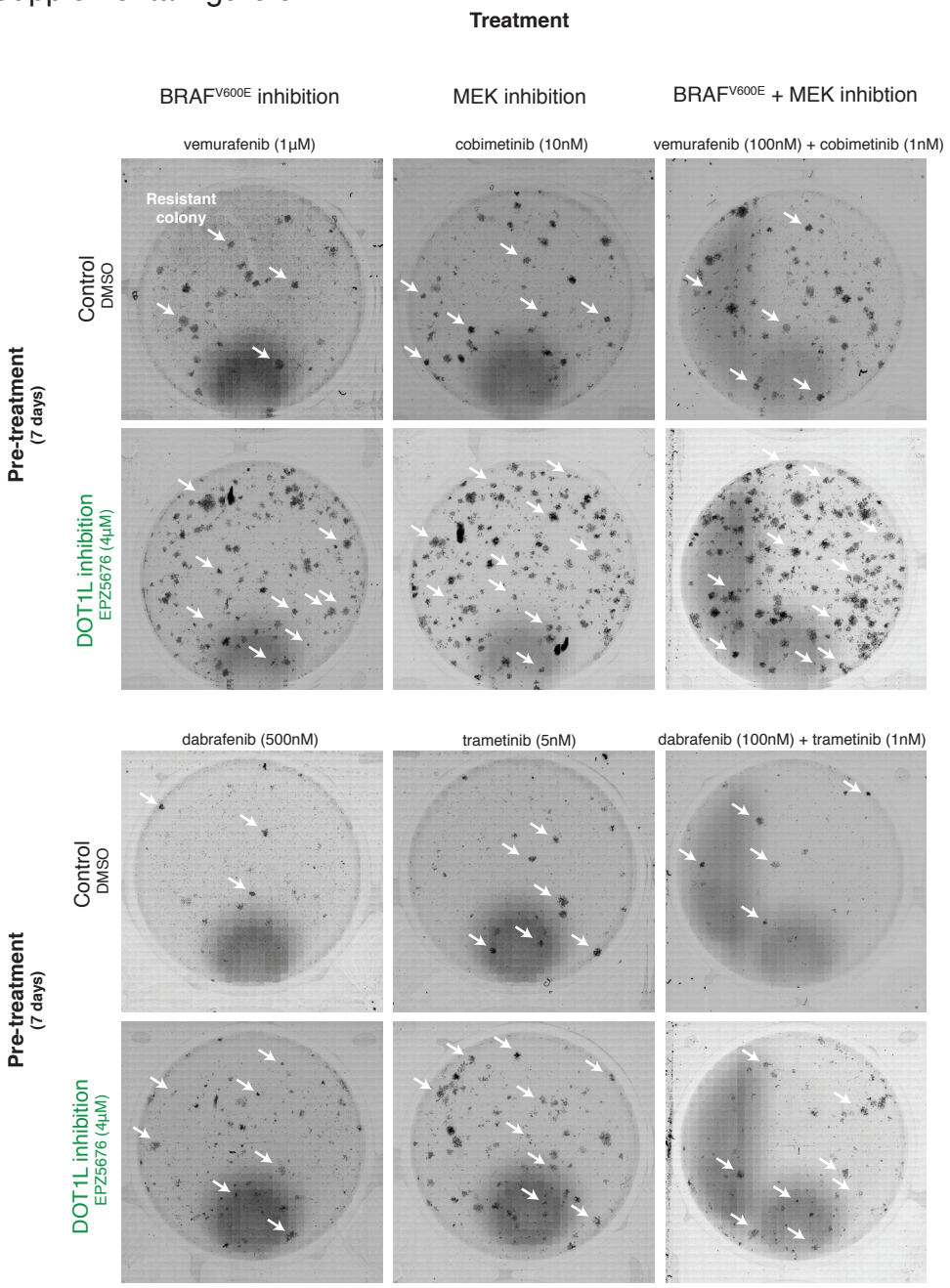

Supplemental figure 10

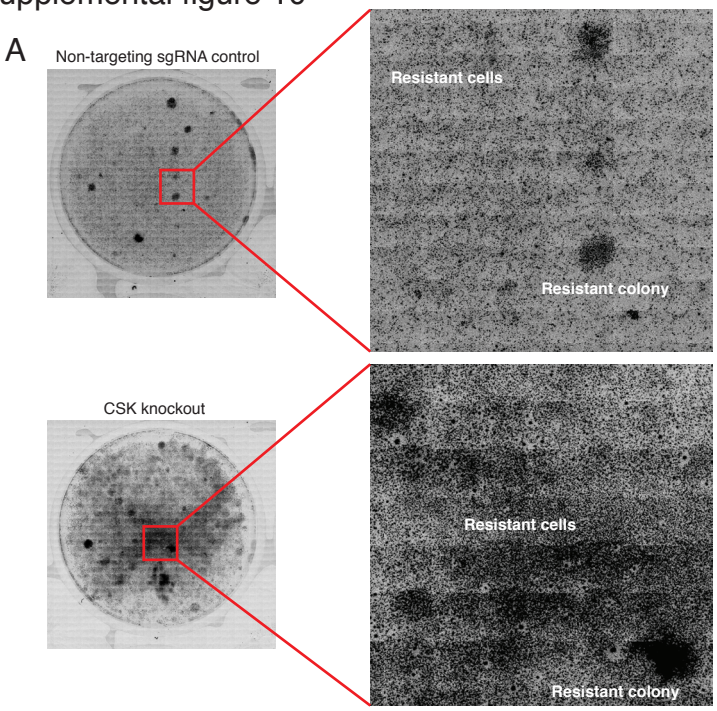

Supplemental figure 11

Bicluster of CRISPR hits based on all differentially expressed genes

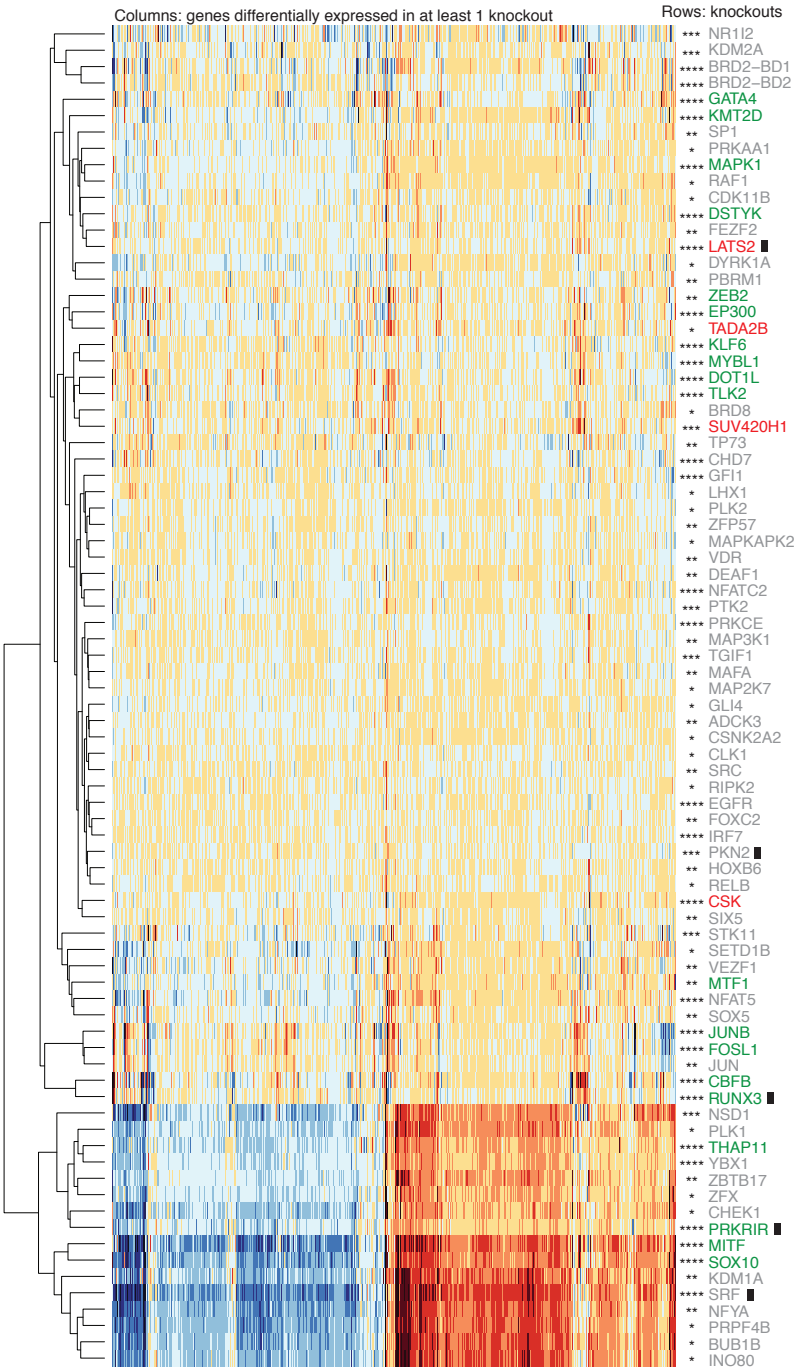

Heatmap color key

$\log_2$ fold change over non-targeting sgRNA control

–3 –2 –1 0 1 2 3

Knockout color key

sgRNA representation in primary state screen

sgRNAs enriched in NGFR^{HIGH}/EGFR^{HIGH} cells

sgRNAs enriched in cells resistant to vemurafenib

sgRNAs depleted in NGFR^{HIGH}/EGFR^{HIGH} cells OR in cells resistant to vemurafenib

% of sgRNAS exhibiting a two-fold change or more

**** Tier 1: ≥75% of the sgRNA exhibited ≥ two-fold change in the primary screen

*** Tier 2: ≥66%

** Tier 3: ≥50%

* Tier 4: ≤50%

▮ These targets are tier 1 or tier 2 in both screens

Supplemental figure 12
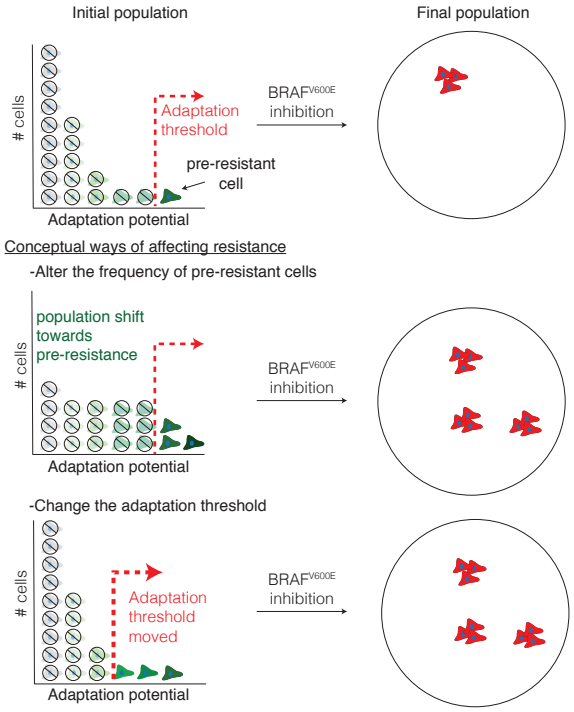
The number of pre-resistant cells beyond a population's adaptation threshold determines the the number of cells that survive the drug